MAPPING CHANGES OF MIRNA-MRNA NETWORKS IN *LEISHMANIA-INFECTED* MACROPHAGES PREDICTS REGULATORY MIRNA-TF LOOPS AS NOVEL TARGETS OF PARASITE IMMUNE SUBVERSION

Charfeddine Gharsallah[1,4], Hervé Lecoeur[1], Hugo Varet[2,3], Rachel Legendre[2,3], Odile Sismeiro[3], Jean-Yves Coppée[3], Caroline Proux[3], Elisabetta Scarfiello[5], Astrid Bruckmann[5], Gunter Meister[5], Eric Prina[1], and Gerald F. Späth[1]

[1]Institut Pasteur, Université Paris Cité, INSERM U1201, Unité de Parasitologie Moléculaire et Signalisation, 25 Rue du Dr Roux, 75015 Paris, France; [2]Institut Pasteur, Université Paris Cité, Hub Bioinformatique et Biostatistique, 28 Rue du Dr Roux, 75015 Paris, France ; [3]Institut Pasteur, Université Paris Cité, Plate-forme Technologique Biomics, Centre de Ressources et Recherches Technologiques (C2RT), 28 Rue du Dr Roux, 75015 Paris, France. [4] Université de Tunis El Manar, Institut Pasteur de Tunis, LR11IPT02 Laboratory of Transmission, Control and Immunobiology of Infections (LTCII), Tunis, Tunisia; [5]Regensburg Center for Biochemistry (RCB), Laboratory for RNA Biology, University of Regensburg, 93053 Regensburg, Germany.

*Correspondance: gerald.spaeth@pasteur.fr

Keywords: *Leishmania*, macrophage infection, host-parasite interaction, epigenetics, microRNA, immune subversion, differential expression, network analysis.

Abstract

MicroRNAs (miRNAs) are small non-coding RNAs that regulate gene expression at the post-transcriptional level and play a crucial role in numerous disease processes, including infections. Although intracellular microbial pathogens are known to modulate host cell gene expression to establish permissive conditions for infection, the specific role of host-encoded miRNAs underlying such subversion remains poorly understood. In this study, we employed the protozoan parasite *Leishmania amazonensis* as a model system to investigate how infection of macrophages modifies the host cell miRNA profile to evade antimicrobial functions and to establish permissive conditions for intracellular proliferation. Dual RNA-seq analyses using matched mRNA and miRNA-enriched samples from uninfected and *L. amazonensis*-infected bone marrow-derived macrophages (BMDMs) revealed 102 differentially expressed miRNAs (padj<0.05), with 18 miRNAs showing reduced and 84 miRNAs showing increased abundance in infected BMDMs. Mapping putative networks of miRNA-mRNA interactions based on the observed expression changes, combined with Gene Ontology enrichment analyses, allowed us to identify potential miRNA target genes involved in key biological processes and metabolic pathways that permit parasite intracellular survival and proliferation. Our analyses predict the existence of a large miRNA-mRNA network affecting the expression level of numerous transcription factors that indicates inhibition of the NF-κB-dependent inflammatory response or the promotion of cholesterol biosynthesis during infection. In particular, the over 10e3-fold increase in the abundance of mmu-miR-686 in infected BMDMs was correlated with a reduced abundance of putative target transcripts implicated in miRNA biogenesis itself, in RNA binding, and in regulation of apoptosis, such as *Caspase 12*, the mRNA decay activator protein *Zfp36l1* or *Leukemia Inhibitory Factor Receptor Alpha*. Likewise, the over 200-fold increase in abundance of mmu-miR-6546-3p was associated with a reduced abundance of putative target mRNAs implicated in cytokine-mediated signaling, positive regulation of apoptotic process and regulation of gene expression, affecting, for example, the *MADS box transcription enhancer factor 2*, the *transformation related protein 53 inducible nuclear protein 1*, or the *G protein-coupled receptor 35*. Interestingly, both miRNAs are predicted to simultaneously target 32 mRNAs that showed reduced abundance in infected BMDMs, including *Maturin Neural Progenitor Differentiation Regulator* (*Mturn*), a regulator of NF-κB transcription factor activity. In conclusion, our approach provides novel insight into molecular mechanisms that may govern macrophage subversion and intracellular *Leishmania* survival. Our results shed new

light on the complex relationship among miRNAs, macrophage gene expression and *Leishmania* infection, proposing regulatory feed-forward loops (FFLs) and feedback loops (FBLs) between miRNAs and TFs as a novel target of *Leishmania* immune subversion. These findings open exciting new avenues for the development of intervention strategies aimed at disrupting such crucial interactions, for example using an anti-miR (antagomir) approach against mmu-miR-686 and mmu-miR-6546-3p.

62 **INTRODUCTION**

63 Epigenetic regulation is a complex mechanism that fine-tunes eukaryotic gene expression. Among
64 epigenetic factors, microRNAs (miRNAs) have emerged as key molecules, intervening at the post-
65 transcriptional level by targeting specific messenger RNAs (mRNAs) to modulate gene expression.
66 Their implications extend to a wide range of human diseases, encompassing areas as diverse as
67 cancer and microbial infections (Atri et al., 2019; Zhang et al., 2019). The importance of miRNAs
68 lies in their ability to act as subtle regulators, actively participating in the precise adjustment of
69 protein levels in cells. This regulation is crucial for maintaining cellular homeostasis and for the
70 adaptive response to environmental challenges (Sprenkle et al., 2023). However, the influence of
71 miRNAs is not limited to normal gene regulation. Indeed, they play a leading role in the context of
72 microbial infections, where pathogens - whether viral, bacterial, or eukaryotic - have developed
73 sophisticated epigenetic mechanisms to disrupt gene expression within host cells, thus ensuring
74 their survival and replication (Ahluwalia et al., 2017; Sun et al., 2017). One of the strategies favored
75 by these pathogens is the modulation of the expression of host miRNAs.

76 *Leishmania* are protozoan parasites that infect mammalian macrophages, inducing a significant
77 disruption of the functions of these cells, leading to severe immune pathologies known as
78 "leishmaniases" (Conceicao-Silva and Morgado, 2019; McGwire and Satoskar, 2014). The
79 consequences of this immune subversion are varied, ranging from self-healing cutaneous forms to
80 potentially fatal visceral forms. However, despite the magnitude of the public health problems
81 posed by leishmaniasis and the profound impact of *Leishmania* infections on the physiology of
82 host cells, the precise mechanisms of this immune subversion remain incompletely understood.

83 Recently, epigenetic subversion has emerged as a major strategy that these parasites use to escape
84 host defenses (Gutierrez Sanchez et al., 2023; Kamhawi and Serafim, 2020; Lecoeur et al., 2022a).
85 First, *Leishmania* infection has been correlated to changes in host miRNA abundance, known to
86 limit the expression of pro-inflammatory genes, thus favoring parasite survival (Ganguly et al.,
87 2022; Lemaire et al., 2013; Mukherjee et al., 2015; Muxel et al., 2018; Nandan et al., 2021; Tiwari
88 et al., 2017). Second, intracellular infection by *Leishmania* causes important changes in the
89 macrophage DNA methylation pattern, affecting signaling pathways, oxidative phosphorylation,
90 and cell adhesion (Marr et al., 2014). Finally, we have previously provided the first evidence that

91 *Leishmania* also manipulates the histone code of the host cell both *in vitro* and *in vivo*, causing
92 hypo-methylation and hypo-acetylation at promoters of pro-inflammatory genes that correlated
93 with reduced gene expression (Lecoeur et al., 2020a).

94 Here, we performed a dual RNAseq analysis to simultaneously profile changes in mRNA and
95 miRNA abundances in primary, bone marrow-derived macrophages infected with lesion-isolated
96 *L. amazonensis* amastigotes (Fernandes et al., 2022; Lecoeur et al., 2022b; Lemaire et al., 2013;
97 Martinez-Hernandez et al., 2021; Rashidi et al., 2021). Computational analysis of these data sets
98 allowed us to map putative miRNA-mRNA regulatory networks that are predicted to control the
99 observed inhibition of the pro-inflammatory TLR / NF-κB signalling pathway and increased
100 cholesterol biosynthesis, both of which are prerequisites for intracellular parasite survival
101 (Gutierrez Sanchez et al., 2023; Lecoeur et al., 2020a). Our findings open new perspectives for
102 anti-parasitic intervention targeting the non-coding transcriptome of the host cell.

103 **MATERIAL AND METHODS**

104 **Ethics statement**

105 Six-week-old female C57BL/6JRj and Swiss nu/nu mice were purchased from Janvier (Saint
106 Germain-sur-l'Arbresle, France). All animals were housed in A3 animal facilities according to the
107 guidelines of Institut Pasteur and the "Comité d'Ethique pour l'Expérimentation Animale" (CEEA)
108 and protocols were approved by the "Ministère de l'Enseignement Supérieur, Direction Générale
109 pour la Recherche et l'Innovation" under number 2013-0047. EP is authorized to perform
110 experiments on vertebrate animals (license 75–1265) issued by the 'Direction Départementale de
111 la Protection des Populations de Paris' and is responsible for all the experiments conducted
112 personally or under his supervision as governed by the laws and regulations relating to the
113 protection of animals.

114

115 **Bone marrow-derived macrophages**

116 Bone marrow cell suspensions were recovered from tibias and femurs of female C57Bl/6JRj mice
117 in Dulbecco's phosphate buffered solution (PBS), and cultured in complete medium containing 4
118 g/L glucose, 1 mM pyruvate and 3.97 mM L-Alanyl-L-Glutamine and supplemented with 10%
119 heat-inactivated fetal calf serum (FCS), streptomycin (50 µg/mL), and penicillin (50 IU/mL)
120 (Sigma-Aldrich, P4333) and 50 µM β-mercaptoethanol (Sigma-Aldrich, M7522), (de La Llave et
121 al., 2011). Briefly, one million cells per ml of complete medium supplemented with 50 ng/ml of
122 mouse recombinant colony-stimulating factor 1 (rm-CSF1, ImmunoTools) were incubated in
123 bacteriological Petri dishes (Greiner bio-one 664161) at 37°C in 7.5% CO_2 atmosphere. After 6
124 days of culture, the medium was removed and adherent cells were incubated with pre-warmed PBS
125 pH 7.4 containing 25 mM EDTA for 30 min at 37°C. Bone marrow-derived macrophages
126 (BMDMs) were detached by gentle flushing, collected, and resuspended in a complete medium
127 supplemented with 30 ng/ml of rmCSF-1. BMDMs were seeded in 100 mm tissue culture dishes
128 (Petri BD Falcon, 353003) for nuclear or total protein extraction and RNA isolation.

129

130 **Parasite isolation and macrophage infection**

131 mCherry-transgenic, tissue-derived amastigotes of *Leishmania amazonensis* strain LV79 (WHO
132 reference number MPRO/BR/72/M1841) were isolated from infected footpads of Swiss nude mice
133 (Lecoeur et al., 2020a). After seeding at day 6 of differentiation, BMDMs were left for 5 hours at
134 37°C to attach to their new culture support. BMDMs were infected with lesion-derived *L.*
135 *amazonensis* amastigotes at a multiplicity of infection (MOI) of 4 and then cultured at 34°C. These
136 cells were referred to as Infected Macrophages (IMs) versus un-infected BMDMs (UIMs).

137

138 **RNA extraction**

139 Large and small (including miRNAs) RNA fractions were isolated from the same macrophage
140 samples using the NucleoSpin miRNA kit (Macherey-Nagel) according to the manufacturer's
141 instructions. Evaluation of RNA quality was carried out by optical density measurement using a
142 Nanodrop device (Kisker, http://www.kisker-biotech.com). RNAs were isolated from 3
143 independent biological replicates of UIMs and IMs at 48 hours post-infection (PI).

144

145 **RNA-Seq analysis**

146 Library preparation and sequencing was performed at the Biomics platform of Institut Pasteur.
147 mRNA processing: Briefly, DNAse-treated RNA extracts from Large RNA fractions were
148 processed for library preparation using the Truseq Stranded mRNA sample preparation kit
149 (Illumina, San Diego, California) according to the manufacturer's instructions. An initial poly A+
150 RNA isolation step (included in the Illumina protocol) was performed with 1 µg of large RNA to
151 isolate the mRNA fraction and remove ribosomal RNA. The mRNA-enriched fraction was
152 fragmented by divalent ions at high temperatures. The fragmented samples were randomly primed
153 for reverse transcription followed by second-strand synthesis to create double-stranded cDNA
154 fragments. No end repair step was necessary. An adenine was added to the 3'-end and specific
155 Illumina adapters were ligated. Ligation products were submitted to PCR amplification. The quality
156 of the obtained libraries was controlled using a Bioanalyzer DNA1000 Chips (Agilent, # 5067-
157 1504) and quantified by spectrofluorimetric analysis (Quant-iT™ High-Sensitivity DNA Assay
158 Kit, #Q33120, Invitrogen). Sequencing was performed on the Illumina Hiseq2500 platform to
159 generate single-end 65 bp reads bearing strand specificity. Reads were cleaned using cutadapt

160 version 1.11 and only sequences at least 25 nt in length were considered for further analysis. STAR
161 version 2.5.0a (Dobin et al., 2013), with default parameters, was used for alignment on the
162 reference genome (GRCm38 from Ensembl database 94). Genes were counted using featureCounts
163 version 1.4.6-p3 (Liao et al., 2014) from the Subreads package (parameters: -t gene -s 0).

164 miRNA processing: Sequencing was performed on the Illumina Hiseq2500 platform to generate
165 single-end 50 bp reads with strand specificity. Reads were cleaned using cutadapt version 1.11,
166 and only sequences with a length between 18 and 28 nucleotides were considered for further
167 analysis. UMIs were added to read headers using umi-tools extract version 1.0.0 (Smith et al.,
168 2017). Bowtie version 1.2.2 (Langmead et al., 2009), with default parameters, was used for
169 alignment to the reference genome (GRCm38 from Ensembl database 92). Reads were
170 deduplicated using umi-tools dedup to remove genuine PCR duplicates identified by UMIs.
171 miRNAs were counted using featureCounts version v1.6.1(Liao et al., 2014) from the Subreads
172 package (parameters: t miRNA -g Name -s 1) and the annotation from mirBase.

173 The data are publicly available at the NCBI's Gene Expression Omnibus repository (ongoing
174 Superseries submission).

175

176 RNA-seq data analyses: Count data were analyzed using R version 3.6.1 (R-Core-Team, 2016) and
177 the Bioconductor package DESeq2 version 1.24.0 (Love et al., 2014). The normalization and
178 dispersion estimation were performed with DESeq2 using the default parameters and statistical
179 tests for differential expression were performed applying the independent filtering algorithm. A
180 generalized linear model was set in order to test for the differential expression between the
181 conditions For each pairwise comparison, raw p-values were adjusted for multiple testing
182 according to the Benjamini and Hochberg (BH) procedure (Benjamini and Hochberg, 1995) and
183 genes with an adjusted p-value lower than 0.05 were considered differentially expressed.

184

185 **Construction of putative miRNA/mRNA genetic interaction networks**

186 To identify potential miRNA targets, we adopted an approach integrating computational prediction
187 methods and experimental data, based on simultaneous profiling of miRNA and mRNA expression
188 changes in our experimental system. Potential targets of differentially expressed miRNAs were

189 predicted as follows: For each differentially regulated miRNA, putative target mRNAs were first
190 selected based on their inverse, differential expression during infection, considering an adjusted p-
191 value of less than 0.05 as statistically significant for both miRNA and mRNA signals. We next
192 employed the TargetScan (version 7.2) (https://www.targetscan.org/mmu_72/) (Agarwal et al.,
193 2015; McGeary et al., 2019) and miRDB (http://www.mirdb.org/mirdb/index.html) (Chen and
194 Wang, 2020) tools associated with the miRbase database (v22) (https://mirbase.org/search/)
195 (Griffiths-Jones et al., 2006; Kozomara et al., 2019) to screen for interactions between miRNAs
196 and target mRNAs based on sequence complementarity. These putative associations were then
197 visualized utilizing the Cytoscape software package (version 3.10.0) (Shannon et al., 2003), with
198 each node of the predicted miRNA-mRNA networks colored based on the differential expression
199 value (blue, decreased abundance; red, increased abundance).

200 Secondary structures and thermodynamic stability of prioritized miRNA sequences were predicted
201 using the RNAfold web server (http://rna.tbi.univie.ac.at/cgi-bin/RNAWebSuite/RNAfold.cgi)
202 (Lorenz et al., 2011). Additionally, we employed the RNAcomposer web server
203 (http://rnacomposer.ibch.poznan.pl/) (Popenda et al., 2012) to predict the 3D structure of
204 prioritized miRNAs. Visualization of these three-dimensional structures was performed using the
205 BIOVIA Discovery Studio Visualizer software (https://discover.3ds.com/discovery-studio-
206 visualizer-download). To determine the minimal free hybridization energy of these miRNAs with
207 select potential targets, we utilized the RNAhybrid web server (https://bibiserv.cebitec.uni-
208 bielefeld.de/rnahybrid) (Kruger and Rehmsmeier, 2006).

209

210 **Gene ontology and pathway analyses**

211 Gene Ontology (GO) term enrichment analyses were conducted for all mRNAs showing
212 differential expression between uninfected (UIM) and infected (IM) macrophages ($p < 0.05$),
213 utilizing the GoTermFinder platform (http://www.go.princeton.edu/cgi-bin/GOTermFinder).
214 Subsequently, the REVIGO Web server (http://www.revigo.irb.hr/) was employed to generate GO
215 scatter plots, using the default list size (Medium: 0.7) (Supek et al., 2011). The associated values
216 for each GO term represent the P-value, which is also reflected by the intensity of the bubble color.
217 Bubble size indicates the frequency of the GO term in the underlying GO annotation (GOA)

218 database (bubbles of more general terms are larger). Obsolete GO terms were removed, and SimRel
219 (default) settings was applied to measure semantic similarity.

220 GO terms enrichment analyses of differentially expressed miRNAs between uninfected (UI) and
221 infected (I) macrophages ($p < 0.05$) was performed using the miEAA platform (https://ccb-
222 compute2.cs.uni-saarland.de/mieaa/) that integrates data from different databases, such as miRBase,
223 miRWalk et miRTarBase (Backes et al., 2016). miEAA is tailored for miRNA precursors and
224 mature miRNAs from several frequently studied species, such as human, mouse, or rat.
225 Subsequently, GO scatter plots were visualized using the REVIGO Web server as detailed above.

226 Gene lists used in our analyses were downloaded from the databases KEGG (Kyoto Encyclopedia
227 of Genes and Genomes, https://www.kegg.jp/kegg/) and MGI (Mouse Genome Informatics,
228 https://www.informatics.jax.org/), while the list of experimentally validated transcription factors was
229 used as published by Lambert and colleagues (Lambert et al., 2018). The resulting gene lists were
230 then analyzed for possible miRNAs target sites using the TargetScan platform (version 7.2)
231 (https://www.targetscan.org/mmu_72/), which predicts potential mRNA targets of canonical
232 miRNAs by searching for the presence of 8mer, 7mer, and 6mer sites complementary to the seed
233 region for a given miRNA (Agarwal et al., 2015; Riolo et al., 2020). The 6mer corresponds to a
234 perfect sequence of 6 nucleotides with the seed region of the miRNA (miRNA nucleotides 2 to 7)
235 (Lewis et al., 2005). The most optimal 7mer site, referred to as 7mer-m8, features a match with the
236 seed region strengthened by a pairing with the 8th nucleotide of the miRNA (Brennecke et al.,
237 2005; Krek et al., 2005; Lewis et al., 2005; Lewis et al., 2003). Another 7mer site, 7mer-A1, is also
238 effective as it includes a seed match with an 'A' at target position 1 (Lewis et al., 2005). Lastly, the
239 8mer site consists of a seed match flanked by a match at position 8 and a match with an 'A' at
240 position 1 (Lewis et al., 2005). Our miRNA-mRNA interaction networks were further refined using
241 the TargetScan parameter 'site types' (8mer, 7mer-m8, 7mer-1A, and non-canonical pairing) and
242 the number of sites in all annotated 3′ UTRs. This parameter selection is based on the notion that
243 among the presented motifs, the greater the number of nucleotides involved in pairing, the more
244 effective the interaction will be. Thus, the type of site (e.g., whether the site is an 8mer or 7mer-
245 m8) strongly influences repression efficacy. The number of sites also influences efficacy, with each
246 additional site typically acting independently to confer additional repression, although sites situated
247 between 8 and 40 nt from each other tend to act cooperatively (Agarwal et al., 2015; Grimson et

248 al., 2007). This approach facilitates direct comparison with other studies employing TargetScan
249 and ensures the reproducibility of our results.

250

251 **Ago-APP**

252 Ago-APP (Ago Affinity Purification by Peptides) was essentially carried out as described earlier
253 in (Hauptmann et al., 2015). Briefly, per 50 µL of anti-FLAG-M2 agarose (Sigma-Aldrich), a
254 minimum of 100 µg FLAG-tagged peptide (TNRC6B 599–683) was coupled to the beads for 3 h
255 at 4 °C. Excess peptide was removed by washing with PBS three times, and lysate was added to
256 the peptide-coupled beads. After incubation for 3 h at 4 °C, the beads were washed four times with
257 NET buffer (50 mM Tris, pH 7.5, 150 mM NaCl, 5 mM EDTA, 0.5 % Nonidet P-40, 10 %
258 glycerol, 1 mM NaF; supplemented with 0.5 mM DTT and 1 mM AEBSF before use) and once
259 with PBS. The beads were eluted by addition of 2× Laemmli sample buffer and incubation at 95 °C
260 for 5 min.

261

262 **Phosphosite measurements by mass spectrometry**

263 Phosphosite measurements of Ago2 proteins by mass spectrometry were performed as described
264 earlier in (Quevillon Huberdeau et al., 2017). SDS-gel bands of affinity-purified Ago proteins were
265 excised, transferred into 2ml micro tubes (Eppendorf), washed with 50 mM NH_4HCO_3, 50 mM
266 NH_4HCO_3/acetonitrile (3/1), 50 mM NH_4HCO_3/acetonitrile (1/1) and lyophilized. After reduction
267 and alkylation of cysteines with DTT and Iodoacetamide, gel slices were again washed as described
268 above and lyophilized. Proteins were subjected to *in gel* tryptic digest overnight at 37 °C with
269 approximately 2 µg trypsin per 100 µl gel volume (Trypsin Gold, mass spectrometry grade,
270 Promega). Peptides were first extracted with 100 mM NH_4HCO_3, followed by 50 mM NH_4HCO_3
271 in 50 % acetonitrile. Combined eluates were lyophilized and reconstituted in 20 µl 1 % TFA prior
272 to LC-MS/MS. Separation of peptides by reversed-phase chromatography was carried out on an
273 UltiMate 3000 RSLCnano System (Thermo Fisher Scientific, Dreieich) which was equipped with
274 a C18 Acclaim Pepmap100 preconcentration column (100 µm i.D.x20 mm, Thermo Fisher
275 Scientific) followed by an Acclaim Pepmap100 C18 nano column (75 µm i.d.x250 mm, Thermo
276 Fisher Scientific). A linear gradient of 4 % to 40 % acetonitrile in 0.1 % formic acid over 60 min

277 was used to separate peptides at a flow rate of 300 nl/min. Via a CaptiveSpray nanoflow
278 electrospray source the LC was coupled to a maXis plus UHR-QTOF System (Bruker Daltonics,
279 Bremen). Data-dependent acquisition of MS/MS spectra by CID fragmentation was performed at
280 a resolution of minimum 60000 for MS and MS/MS scans. The MS spectra rate of the precursor
281 scan was 2 Hz processing a mass range between m/z 175 and m/z 2000. Via the Compass 1.7
282 acquisition and processing software (Bruker Daltonics) a dynamic method with a fixed cycle time
283 of 3 s and an m/z dependent collision energy adjustment between 34 and 55 eV was applied. Raw
284 data processing was performed in Data Analysis 4.2 (Bruker Daltonics). ProteinScape 3.1.3
285 (Bruker Daltonics) in connection with Mascot 2.5.1 (Matrix Science) facilitated database
286 searching. The following search parameters were applied: database Swiss-Prot *Mus musculus*,
287 enzyme specificity trypsin with 2 missed cleavages allowed, precursor tolerance 0.02 Da, MS/MS
288 tolerance 0.04 Da, variable modifications: acetylation at protein N-terminus,
289 carbamidomethylation and propionamide modification of cysteine, oxidation of methionine,
290 deamidation of asparagine and glutamine, phosphorylation of serine, threonine and tyrosine.
291 Mascot peptide ion-score cut-off was set 15. Phosphopeptide fragment spectra were evaluated
292 manually. Calculation of relative abundances of phosphopeptide species at the S825-S835
293 phospho-cluster was based on peptide intensities. The sum of peptide intensities of all peptide
294 species detected at the cluster position was considered as 100 %. Peptide intensities of individual
295 phosphorylated or non-phosphorylated species were then used to determine the relative abundance
296 of each peptide as a percentage.

297

298

299 **RESULTS AND DISCUSSION**

300

301 ***L. amazonensis* infection modulates expression of RISC components and Ago2**
302 **phosphorylation.** Argonaute (Ago) proteins are fundamental regulators of mammalian gene
303 expression (Mauro et al., 2023). As key components of the RNA-induced silencing complex
304 (RISC), they are essential in mediating the functions of microRNAs (miRNAs), a class of non-
305 coding RNAs that regulate gene expression at the post-transcriptional level promoting mRNA
306 degradation or inhibiting protein translation (Larivera et al., 2023) (Figure 1A). The dysregulation

307 of RISC functions has been implicated in a wide range of pathologies – including microbial
308 infection - revealing miRNAs as promising therapeutic targets for RNA-based intervention
309 strategies (Li et al., 2014). However, how pathogenic microbes exploit the Ago/RISC/miRNA axis
310 to reprogram their host cells is only poorly understood. Here we use the protozoan parasite
311 *Leishmania* as a unique model system to address this major scientific gap and gain mechanistic
312 insight into how these human pathogens manipulate miRNA networks to subvert host defenses and
313 ensure their own survival.

314 Drawing from previously published RNAseq analyses of *L. amazonensis*-infected, bone
315 marrow-derived macrophages (BMDMs), we first investigated expression changes of the RISC
316 members and associated proteins indicated in Figure 1A. Significant expression changes compared
317 to uninfected BMDMs ($p < 0.05$) were observed for major RISC components (Figure 1B),
318 including (i) the Argonaute family member Ago2 (over 5-fold increase), a multifunctional
319 scaffolding protein that confers miRNA silencing, or (ii) the RNA-binding protein ZFP36L1 binds
320 adenylate-uridylate-rich elements (AREs) in the 3'UTRs of mRNAs, recruiting the CCR4-NOT
321 deadenylase complex to remove poly(A) tails, leading to mRNA degradation (Loh et al., 2020).

322 Ago proteins are phosphorylated at different residues and specific functions have been
323 assigned to these modifications (Golden et al., 2017; Hauptmann et al., 2015; Quevillon Huberdeau
324 et al., 2017). Whether *Leishmania* infection alters such phosphorylation patterns, however, has not
325 been investigated. Therefore, we isolated all four murine Ago proteins from *Leishmania*-infected
326 BMDMs using the AgoAPP approach (Hauptmann et al., 2015) and analyzed phosphorylation
327 patterns by mass spectrometry (Figure 1C). Indeed, phosphorylation of serine 388 (S388), which
328 was associated with specific sub-cellular Ago localization patterns (Zeng et al., 2008), was strongly
329 reduced upon infection (Figure 1C, left panel). Ago proteins undergo a phosphorylation cycle
330 involving a hypo- and hyper-phosphorylation of a C-terminal Ser/Thr cluster (Golden et al., 2017;
331 Quevillon Huberdeau et al., 2017). Depending on the amount of the negative charge that is added
332 by phosphorylation to this cluster, mRNA binding of Ago/miRNA complex is inhibited. While
333 single phosphorylation events at Ser825 are not significantly changed upon infection (Figure 1C,
334 middle panel), peptides that carry double phosphorylations at S825 and S829 are clearly increased
335 during *Leishmania* infection (Figure 1C, right panel).

336 In conclusion, *Leishmania* has a profound effect on the expression of RISC components in
337 infected macrophages that on one hand triggers increased expression of Ago2, while on the other
338 hand balancing its functions by Ago2 hyper-phosphorylation to reduced Ago/miRNA activity.
339 These results primed us to directly investigate changes of the miRNA landscape during infection.

340

341 ***L. amazonensis* subverts both the mRNA and miRNA landscapes in infected BMDMs.**
342 Changes in miRNA and mRNA abundances were investigated in uninfected, bone marrow-derived
343 macrophages (BMDMs, referred to as UIMs) and *L. amazonensis* infected BMDMs (referred to as
344 IMs) established using virulent, lesion-derived amastigotes (Figure 2). Large (mRNAs) and small
345 (primarily miRNAs) RNA fractions were isolated from these samples at day 2 post-infection (PI)
346 and subjected to RNAseq analysis (Figure 2A). As judged by the expression changes observed
347 across three independent biological replicates, *Leishmania* infection has a major impact on both
348 the mRNA and miRNA profiles of IMs, with significant changes observed for the abundance of
349 5742 mRNAs (10.36 % of total, padj <0.05) and 102 miRNAs (6.04 % of total, padj <0.05) (Figure
350 2B1 and 2C1). Inspection of biological functions enriched in the differentially expressed genes
351 (Figure 2B2) and miRNAs (Figure 2C2), revealed a series of GO terms that were previously
352 associated with *Leishmania*-mediated immune subversion and infected macrophages and that
353 converged in both the miRNA and mRNA datasets, including GO terms linked to inflammatory
354 response, NF-κB signaling, apoptosis, or essential metabolic processes related to cholesterol and
355 fatty acid biosynthesis (Figures 2B2 and C2).

356 Closer inspection of miRNA read depth variations during infection identified 84 miRNAs
357 (82.4%) with and 18 miRNAs (17.6%) with decreased abundance, suggesting that intracellular *L.*
358 *am* has a profound effect on the miRNA landscape in agreement with a previously published report
359 using *L. amazonensis* infected BMDMs from BALB/c (Muxel et al., 2017) (Figure 2D1 and D2,
360 respectively). Important read depth variations were observed for mmu-miR-686 that showed an
361 over 1000-fold increase in abundance (3 normalized reads in UIMs vs 3953 in IMs), as well as for
362 mmu-miR-6546-3p (2 vs 891, 445-fold increase) and mmu-miR-718 (261vs 1,023, 3.9-fold
363 increase) (Figure 2D1). Significant increase in expression was further observed for a series of
364 murine miRNAs with high homology to human (https://rnacentral.org/), such as mmu-miR-150-
365 3p, mmu-miR-488-3p, and mmu-miR-299a-5p. In contrast, the strongest reduction in read depth

366 during infection was observed for mmu-miR-342-3p (55,522 vs 31,602), mmu-let-7b-5p (11,428
367 vs 7,176), mmu-miR-99b-5p (4,508 vs 1,926), mmu-miR-92a-3p (2,278 vs 611), mmu-miR-339-
368 5p (1,271 vs 469), and mmu-miR-532-3p (741 vs 394). Decreased abundance of mmu-let-7b-5p
369 has been also observed during infection with *L. infantum* and *L. major* in human macrophages
370 (Geraci et al., 2015; Ramos-Sanchez et al., 2022), suggesting a key role of this miRNA in
371 intracellular parasite infection.

372 In conclusion, our data confirm the differential expression of miRNAs during intracellular
373 *Leishmania* infection, which correlated with important expression changes at mRNA levels,
374 suggesting the existence of regulatory miRNA-mRNA networks that may govern the establishment
375 of an immune-compromised host cell phenotype. We next applied a series of computational tools
376 to further assess possible miRNA-mRNA regulatory interactions.

377

378 **Modelling interaction networks related to reduced miRNA expression.** miRNA-mRNA
379 regulatory networks are characterized by reciprocal expression changes between both types of
380 RNA, where increased miRNA usually causes decreased expression of its target mRNA (and *vice*
381 *versa*). We investigated the existence of such networks by first focusing on down-regulated
382 miRNAs whose expression changes are supported by at least 50 normalized reads, and their
383 predicted mRNA targets that show increased abundance during infection (Log2 Fold Change (FC)
384 ≥ 1, $p < 0.05$). Only 2 out of the 18 downregulated miRNAs did not pass this filtering step and
385 were excluded (i.e. mmu-702-3p, mmu-miR-99b-5p). Down-regulation of the remaining 16
386 miRNAs were tightly associated with increased abundance of their predicted target mRNAs as
387 illustrated by the interaction network shown in Figure 3A. Important differences were observed
388 between these networks both with respect to the level of miRNA down-regulation as well as the
389 number of possible target mRNAs (Figure 3A). For example, mmu-miR-532-3p and mmu-miR-
390 342-3p respectively are predicted to target only 5 and 10 transcripts, while on the other extreme,
391 mmu-484 and mmu-767 respectively are predicted to target 136 and 97 transcripts (Figure 3A).
392 Some sets of upregulated transcripts are predicted to be solely under the control of a single miRNA,
393 as illustrated by mmu-767 (74 transcripts), mmu-484 (36 transcripts), mmu-miR-3968 (22
394 transcripts), and mmu-let-7b-5p (8 transcripts). Thus, affecting a single miRNA during intracellular

395 *Leishmania* infection can generate a pleiotropic outcome with important consequences on cellular
396 processes and diverse pathologies (Valinezhad Orang et al., 2014).

397 We next focused on the two miRNAs mmu-let-7b-5p (11,428 in UIMs vs 7,176 normalized
398 read counts in IMs, Log2FC = -0.752) and mmu-miR-342-3p, based on (i) their significant
399 differential read count between UIMs and IMs, (ii) their conservation to human miRNAs
400 (Pasquinelli et al., 2000), https://rnacentral.org/sequence-search/?jobid=c25cc34b-01cf-42ae-
401 a24e-611a1132aa1e), and their involvement in key biological processes, including apoptosis,
402 Jak/Stat signaling, or NF-κB signaling (Cui et al., 2019; Lecoeur et al., 2022b; Taghehchian et al.,
403 2023; Tai et al., 2015; Thammaiah and Jayaram, 2016). Consolidating our target mRNA
404 predictions from TargetScan and miRDB platforms established a list of 192 putative mmu-let-7b-
405 5p mRNA targets showing increased abundance during infection, including *Integrin Beta 3 subunit*
406 (*Itgb3*, Log2 FC = 2.35), *Argonaute RISC Catalytic Component 2* (*Ago2*, Log2 FC = 1.37), *Dual-*
407 *specificity phosphatase 9* (*Dusp9*, Log2 FC = 1.94) (Figure 3A) and 7 mRNAs encoding for
408 transcription factors (TFs) or epigenetic regulators (ERs), *i.e.* *Arid3a*, *E2f6*, *Hmga1*, *Klf8*, *Nr6a1*,
409 *Pbx1*, and *Zfp202* (Figure 3B), which are involved in regulation of proliferation regulation, cell
410 differentiation, DNA structure modification, and cancer-related signaling pathways (Bai et al.,
411 2024; Guo et al., 2023; Kao et al., 2024; Patterson et al., 2008; Trimarchi et al., 2001; Wang et al.,
412 2022; Zhang et al., 2024).

413 Likewise, decreased expression of mmu-miR-342-3p was associated with increased
414 expression during infection of 75 putative mRNA targets, including *Syndecan 1* (*Sdc*1, Log2 FC =
415 2.37), *LDL Receptor Protein 8* (*Lrp*8, Log2 FC = 2.82) (Figure 3A) and 9 TFs/ERs (*Cebpg*, *Gmeb1*,
416 *Jazf1*, *Kmt2a*, *Pou3f1*, *Sox7*, *Tcf12*, *Zbtb21*, and *Zbtb42*) (Figure 3B), which regulate genes
417 involved in several biological processes such as glucocorticoid synthesis, regulated cell death or
418 proteasomal protein degradation (An et al., 2019)

419 Both mmu-let-7b-5p and mmu-miR-342-3p share 12 predicted targets, including *Zinc*
420 *Finger Protein 42* (*Zfp42*) (Log2 FC= 2.537), which shows high base pairing probability that
421 suggests strong binding of both miRNAs (Figure 3C1). Specific interaction between both miRNAs
422 and *Zfp42* mRNA is further supported by the low hybridization energy below -20 kcal/mol and the
423 presence of strong 7mer-m8 and 7mer1A binding properties (Figure 3C2).

424 In conclusion, our analyses reveal the presence of putative miRNA-mRNA networks that
425 may participate in increased gene expression observed during *Leishmania* infection. The
426 identification of *Ago2* as a putative miRNA target further suggests the existence of a regulatory
427 feedback loop during *Leishmania* infection, where miRNAs can affect their own production as seen
428 recently in mammalian development (Liu et al., 2021). Furthermore, the identification of TFs as
429 putative miRNA targets opens the possibility to control macrophage gene expression in a
430 cooperative fashion through feed-forward loops (FFLs) and feedback loops (FBLs) (Shalgi et al.,
431 2007; Tsang et al., 2007).

432

433 **Modelling of interaction networks related to increased miRNA expression.** We next applied
434 the same filtering procedure as indicated above to establish networks between the 84 miRNA
435 showing increased expression during infection and the 199 down-regulated mRNAs (Log2 FC ≤ -
436 0.5). The 33 miRNAs of the network shown in Figure 4A passed this filtering step and were
437 prioritized for network analysis considering the level of their increased expression and their high
438 conservation with human miRNA for some of them. As expected, increased expression of these
439 miRNAs correlated with decreased abundance of their predicted mRNA targets (Figure 4A).
440 Important differences were observed for the number of putative mRNA targets that are predicted
441 to interact with these miRNAs (Figure 4A), with for example mmu-miR-299a-5p predicted to target
442 only *Ring Finger Protein 150* (*Rnf150*), or mmu-miR-6546-3p to target just 9 transcripts (including
443 1 TF), while mmu-miR-7661-5p is predicted to target 93 transcripts (including 6 TFs) (Figure 4A).

444 For subsequent analyses, we focused our attention on two highly expressed miRNAs. First,
445 mmu-miR-686 shows an over 1000-fold increase of abundance during infection and is predicted to
446 target 433 mRNAs that showed statistically significant reduced abundance during infection ($p <$
447 0,05). Putative mRNA targets showing reduced abundance in our analysis include the mRNA
448 decay-activating protein *Zinc Finger Protein 36*, C3H Type (*Zfp36l1*, Log2 FC = -3.12),
449 *Ribonuclease A Family Member K6* (*Rnase6*, Log2 FC = -2.4) or *Caspase 12* (*Casp12*, Log2 FC =
450 -3.34) (Figure 4B) linking this miRNA to key biological processes such as apoptosis, cell
451 proliferation and chromatin binding. MiR-686 has also the potential to negatively regulate the
452 transcripts of 31 transcription factors, including *Elf4*, *Bcl6*, *Stat1*, *Foxo3*, *Hmbox1*, and *Bcl6*

453 (Figure 4B), adding cell proliferation, differentiation, apoptosis and antimicrobial resistance to its
454 putative list of target processes (Lecoeur et al., 2022a; Spath et al., 2009; Xu et al., 2024).

455 Second, mmu-miR-6546-3p shows an over 200-fold increase of abundance during infection
456 and is predicted to target 117 mRNAs that showed statistically significant reduced abundance
457 during infection ($p < 0.05$) (Figure 4B), including *G-protein-coupled receptor 35* (*Gpr35*, Log2
458 FC = -2.54), which facilitates the activity of the C-X-C chemokine receptor (Boleij et al., 2021) or
459 the developmental TFs *MADS box transcription enhancement factor 2* (*Mef2c*, Log2 FC = -2.48)
460 and *transformation-related protein 53-induced nuclear protein 1*, (*Trp53inp1*, Log2 FC = -1.92)
461 (Figure 4B). mmu-miR-6546-3p has further the potential to reduce the expression of 14
462 transcription factors, including *Ets1*, *Foxo3* (implicated in cell death regulation, (Litvak-Greenfeld
463 and Benhar, 2012), *Mef2c*, *Rela*, *Stat2*, and *Stat3* (Figure 4B), some of which were previously
464 linked to *Leishmania* infection, such as *Stat3* (Mishra et al., 2023) or *Rela,* whose mRNA
465 abundance was reduced during *in vitro* and *in vivo L. amazonensis* infection, dampening the TLR
466 / NF-κB / NLRP3 pathway (Lecoeur et al., 2020a).

467 Both miRNAs have the potential to synergize for the negative regulation of 34 common
468 mRNA targets, including the TFs *Maturin, Neural Progenitor Differentiation Regulator Homolog*
469 (*Mturn*, Log2 FC = -1.559) (Figure 4B). These putative interactions are further supported by (i)
470 strong miRNA-mRNA base pairing probability and an elevated overall thermodynamic free energy
471 of -5.41 (mmu-miR-686) and -1.97 kcal/mol (mmu-miR-6546-3p) (Figure 4C1). In general,
472 miRNAs with high thermodynamic stability are considered crucial for efficient transcriptional
473 regulation, which explains their high intracellular concentrations (>1,000 molecules per cell)
474 according to recent studies (Denzler et al., 2016; Luna et al., 2015). Furthermore, as exemplified
475 by the putative *Foxo3* mRNA target, both miRNAs show a low hybridization energy below -18
476 kcal/mol and the presence of strong 8mer and 7mer1A binding properties (Figure 4C2).

477 In conclusion, just as observed for the $miRNA^{down}/mRNA^{up}$ regulatory networks, the
478 $miRNA^{up}/mRNA^{down}$ regulatory networks described here propose miRNAs as important
479 pleiotropic regulators that may be engaged by *Leishmania* to efficiently reprogram the host cell
480 expression profile in favor of intracellular parasite survival.

481

482 ***In silico* assessment of miRNA-mediated subversion of the TF landscape.** One striking signal
483 emerging from our network analyses is the number of differentially expressed TFs and epigenetic
484 regulators (ERs) that are predicted targets of miRNAs. A focused *in silico* analysis of these
485 interactions is shown in Figure 5 that visualizes simplified networks between 15 down-regulated
486 miRNAs and 79 upregulated TF/ER mRNAs (Figure 5, panel A), and *vice versa* between 34
487 upregulated miRNAs and 160 downregulated, putative TF/ER targets (Figure 5, panel B). These
488 interactions may represent a very cost-efficient parasite immune subversion strategy, where
489 changes in a small set of miRNAs have important consequences on macrophage expression profile
490 and phenotype, either by directly affecting TFs/ERs or by exploiting regulatory feed-forward and
491 feedback loops between miRNAs and TFs/ERs that could jointly control the transcriptomic
492 reprogramming we previously described in *L. amazonensis* infected macrophages and dendritic
493 cells (Lecoeur et al., 2022a; Lecoeur et al., 2020a; Lecoeur et al., 2020b).

494

495 ***In silico* assessment of miRNA-mediated suppression of the pro-inflammatory response.** We
496 have previously identified the TLR / NF-κB axis as a prime target for epigenetic subversion of the
497 macrophage inflammatory response by *L. amazonensis* infection that correlated with histone H3
498 hypo-acetylation and hypo-methylation (Lecoeur et al., 2020a). Our data here uncover that
499 modulation of the host miRNA landscape may constitute an additional epigenetic layer subverting
500 pro-inflammatory signaling during infection. The focused network shown in Figure 6 identifies 16
501 down-regulated miRNAs that are predicted to target 16 up-regulated members of this pathway
502 (panel A), while 28 up-regulated miRNAs are predicted to affect 24 down-regulated pathway
503 members (panel B). Even though this one-on-one regulation may indicate only limited influence
504 of miRNA on expression of these targets, placing these interactions into the context of the entire
505 pathway reveals that miRNAs could affect every step of TLR / NF-κB pathway establishing the
506 anti-inflammatory phenotype characteristic of *Leishmania*-infected macrophages (Figure 6C).
507 miRNA^{up}/mRNA^{down} interactions are observed for a number of activating pathway members, from
508 surface receptors that trigger the initial activation (e.g. miR-138-2-3p for *Cd40*, miR-7088-5p for
509 *Tnfrsf1a*), down to NF-κB family members (miR-6546-3p for *Rela*, miR-546 for *Relb*, miR-299a-
510 5p for *NFkb1*, miR-327 for *Nfkb2*) that induce inflammatory gene expression. On the contrary,
511 miRNA^{down}/mRNA^{up} interactions are observed for deactivating pathway members, such as *Tnfaip3*

512 precited to be targeted by miR-92a-3p. These data reveal miRNAs as potential regulators of the
513 dual inhibition of the macrophage pro-inflammatory response we have described previously
514 (Lecoeur et al., 2020a).

515

516 ***In silico* assessment of miRNA-mediated induction of cholesterol biosynthesis.** Cholesterol
517 biosynthesis represents one of the key biological processes induced during *L. amazonensis*
518 infection believed to be essential for parasite development and vacuole membrane biogenesis
519 (Gutierrez Sanchez et al., 2023; Osorio y Fortea et al.). Our data suggest miRNAs as possible key
520 regulators of this pathway during *Leishmania* infection. The focused network shown in Figure 7
521 identifies 8 down-regulated miRNAs that are predicted to target 32 up-regulated members of this
522 pathway (panel A), while 20 up-regulated miRNAs are predicted to affect 20 down-regulated
523 pathway members (panel B). Placing these putative interactions in the context of the cholesterol
524 pathway (panel C) sheds a more integrative light on the outcome of these transcriptional
525 modulations and again proposes a dual regulation underlying increased cholesterol production.
526 Certain miRNAs act as possible positive regulators of this pathway, with for example down-
527 regulation of miR-532-3p correlating with upregulation of its mRNA target Sterol Regulatory
528 Element Binding Transcription Factor 2 (*Srebf2*), a master regulator of cholesterol biosynthesis
529 (Amemiya-Kudo et al., 2002). In contrast, miRNA^{up}/mRNA^{down} interactions seem to be linked to
530 cholesterol homeostasis, as indicated by down-regulation of the ATP binding cassette subfamily A
531 member *Abca1* (putative target for mmu-miR7661-5p) that functions as a cholesterol efflux pump
532 (Quazi and Molday, 2013), or the cytochrome P450 superfamily member CYP27A1 (putative
533 target for mmu-miR664-3p) controlling cholesterol removal (Pikuleva et al., 1998).Thus the
534 combined effect of these miRNAs likely enhances activating components of cholesterol
535 biosynthesis while at the same time limiting cholesterol removal.

536

537 **CONCLUSION**

538 Applying dual RNAseq analysis on mRNA and miRNA fractions obtained from *L. amazonensis*-
539 infected and uninfected BMDMs allowed us unprecedented insight into the possible role of the
540 host cell noncoding RNome as a novel target for parasite immune subversion. Based on our

541 computational analyses, the observed miRNA expression changes are predicted to affect the
542 abundance of a large array of transcripts that establish the immune-metabolomic expression profile
543 and cellular phenotype characteristic of *L. amazonensis* infected macrophages (Zhang et al., 2022).
544 The challenge for future studies lies on experimentally validating these interactions for example
545 using RNA pull down experiments to establish defined miRNA-mRNA target relationships or
546 applying genetic ablation on key miRNAs to study their effect on host cell gene expression and
547 intracellular parasite survival. These future investigations will hold great promise to define
548 miRNAs as novel, host-directed therapeutic targets against *Leishmania* using agomir and
549 antagomir strategies to restore the anti-microbial potential of host macrophages (Chong et al., 2021;
550 Murdaca et al., 2019; Rupaimoole and Slack, 2017).

551

552 **FIGURE LEGENDS**

553 **FIGURE 1: (A) Schematic overview of the Ago2/RISC/miRNA machinery.** miRNA-loaded
554 Ago2 (RISC) binds TNRC6 (aka GW182) via the interaction between tryptophan (W) binding
555 pockets in AGO and glycine-tryptophan (GW) repeats in TNRC6. TNRC6 destabilizes target
556 mRNAs by recruiting two deadenylation complexes composed of either CAF1-CCR4-NOT1 or
557 PAN2-PAN3, and by recruiting decapping factors, including the decapping enzyme DCP2. Finally,
558 XRN1 degrades the decapped mRNA in a 5′ to 3′ direction. **(B)** Heat map representing the Log2
559 Fold Change values between *L. amazonensis*-infected and uninfected BMDMs at day 3 post-
560 infection. Key components of the Ago2/RISC/miRNA machinery are indicated. Note that Ago2
561 shows a 6-fold induction during infection. **(C)** Phosphorylation analysis of Ago2 protein purified
562 by Ago-APP from *L. amazonensi*s-infected (IMs) vs. uninfected BMDMs (UIMs). LC-MS/MS
563 measurements detected Ago2 phosphorylation changes of serine 388 (left), serine 825 (middle),
564 and serine 825/829 (right). The lower panel shows a schematic view of the Ago2 domain structure,
565 with phosphorylation sites indicated.

566 **FIGURE 2: Dual RNAseq analysis of mRNA and miRNA fractions in *L. amazonensis*-**
567 **infected versus non-infected macrophages. (A)** Experimental pipeline for the generation of
568 BMDMs, their infection, and isolation of large versus small RNAs. BMDMs were derived from
569 mCSF-treated C57BL/6 bone marrow progenitors and were infected (IMs) or not (UIMs) with
570 lesion-derived amastigotes of *L. amazonensis* for 2 days. Large and small RNAs were isolated from
571 the same samples (n=3 independent experiments) and subjected to RNAseq analysis. **(B, C)** Heat
572 maps, volcano plots and REVIGO enrichment maps showing respectively differentially expressed
573 mRNAs and miRNAs across three biological replicates (1-3) in uninfected (UIMs) and infected
574 (IMs) macrophages (B1 and B2, left panels, log2 fold changes (FC) are shown), the distribution of
575 differentially expressed mRNAs and miRNAs according to their average, normalized read counts
576 (B1 and C1, right panels, statistically significant signals with $p < 0.05$ are indicated in red), and
577 biological functions enriched in the datasets of differentially expressed mRNA (B2) and miRNA
578 (C2). Bubble color reflects the p-value of the enrichment and bubble size indicates the frequency
579 of the GO term in the underlying GOA database. For space reasons, only few bubbles are labeled
580 with their corresponding GO term, while others are numbered as follows: 1, Inflammatory response
581 (GO:0006954); 2, Apoptosis process (GO:0006915); 3, Cholesterol homeostasis (GO:0042632);

582 4, Fatty acid biosynthetic process (GO: 0006633); 5, Fatty acid oxidation (GO: 0019395); 6, I-κB
583 kinase/ NF- κB signaling (GO:0007249); 7, Negative regulation of NF- κB TF activity
584 (GO:0032088); 8, Positive regulation of I-κB kinase/ NF-κB signaling (GO:0043123); 9, Response
585 to LPS (GO: 00032496); 10, Response to protozoan (GO:0001562); 11, Macrophage activation
586 (GO: 0042116); 12, Cytokine production involved in immune response (GO:0002367); 13, JNK
587 cascade (GO:0007254); 14, MAPK cascade (GO:0000165); 15, Regulation of gene expression
588 (GO: 0010468); 16, Regulation of DNA-binding TF activity (GO:0051090); 17, Positive regulation
589 of DNA binding (GO:0043388); 19, Chromatin remodelling (GO:0006338); 20, Histone H4
590 acetylation (GO:0043967); 21, Epigenetic regulation of gene expression (GO:0040029); 22,
591 mRNA transport (GO:0051028); 23, RNA-mediated gene silencing (GO:0031047); 24, Positive
592 regulation of miRNA-mediated gene silencing (GO:0043388); 25, miRNA-mediated gene
593 silencing by inhibition of translation (GO:0035278). **(D)** Circular heatmaps of miRNAs showing
594 increased (D1) or decreased (D2) normalized read counts during infection. Highlighted in red and
595 green are miRNAs with high similarity to human miRNAs (except miR-686 and miR6546-3p).
596 Nnr, Normalized read counts.

597 **FIGURE 3: Gene regulatory networks between down-regulated miRNAs and putative target**
598 **mRNAs showing increased abundance in infected macrophages**. **(A)** Predicted interactions are
599 shown between miRNAs (rectangles, fill color indicates level of decreased abundance in log2 FC)
600 and mRNAs (circles, fill color indicates level of increased abundance in log2 FC). Transcription
601 factors are indicated by the oval shape. Shown interactions are based on miRNAs showing a
602 difference of 50 or more normalized reads between infected (IMs) and uninfected (UIMs) groups,
603 and mRNAs showing IMs vs UIMs expression changes of Log2 FC ≥ 1. **(B)** Predicted interaction
604 maps between down-regulated mmu-let-7b-5p and mmu-miR-342-3p and their potential target
605 mRNAs showing increased abundance in IMs vs UIMs. **(C)** 2D and 3D structures of mmu-let-7b-
606 5p and mmu-miR-342-3p (C1). The probability of miRNA binding to the putative target mRNA
607 *Zfp462* is indicated by the color. Target position, length, site type and minimum hybridization
608 energy (mfe) are indicated in panel C2.

609 **FIGURE 4: Gene regulatory networks between up-regulated miRNAs and putative target**
610 **mRNAs showing reduced abundance in infected macrophages**. **(A)** Predicted interactions are
611 shown between miRNAs (rectangles, fill color indicates level of increased abundance in log2 FC)

612 and mRNAs (circles, fill color indicates level of decreased abundance in log2 FC). Transcription
613 factors are indicated by the oval shape. Shown interactions are based on miRNAs showing a
614 difference of 50 or more normalized reads between infected (IM) and uninfected (UIMs) groups,
615 and mRNAs showing IMs vs UIMs expression changes of Log2 FC ≤ -1. **(B)** Predicted interaction
616 maps between up-regulated mmu-686 and mmu-miR-6546-3p and their potential target mRNAs
617 showing decreased abundance in IMs vs UIMs. **(C)** 2D and 3D structures of mmu-686 and mmu-
618 miR-6546-3p (C1). The probability of miRNA binding to the putative target mRNA *Foxo3* is
619 indicated by the color. Target position, length, site type and minimum hybridization energy (mfe)
620 are indicated in panel C2.

621 **FIGURE 5: miRNA network analyses focused on putative mRNA targets implicated in**
622 **expression regulation.** mRNAs encoding for transcription factors (TFs) and epigenetic regulators
623 (ERs) showing significantly increased and decreased abundances (padj < 0.05) are shown in red
624 (panel A) and blue (panel B), respectively. The solid lines (8mer) represent the most efficient
625 interaction. Next are the dashed lines (7mer-m8) and dotted lines (7mer-1A), followed by the sine
626 wave lines (non-canonical), indicating varying levels of interaction efficiency.

627 **FIGURE 6: miRNA network analyses focused on putative mRNA targets implicated in the**
628 **NF-κB pathway.** mRNAs encoding for NF-kB pathway members showing significantly increased
629 and decrease (padj < 0.05) mRNA abundances are shown in red (panel A) and blue (panel B),
630 respectively. The solid lines (8mer) represent the most efficient interaction. Next are the dashed
631 lines (7mer-m8) and dotted lines (7mer-1A), indicating varying levels of interaction efficiency. (C)
632 Projection of miRNA and mRNA expression values and putative regulatory interactions on the NF-
633 κB pathway.

634 **FIGURE 7: miRNA network analyses focused on putative mRNA targets implicated in**
635 **cholesterol biosynthesis and homeostasis.** mRNAs encoding for proteins implicated in
636 cholesterol production showing significantly increased and decrease (padj < 0.05) mRNA
637 abundances are shown in red (panel A) and blue (panel B), respectively. The solid lines (8mer)
638 represent the most efficient interaction. Next are the dashed lines (7mer-m8) and dotted lines
639 (7mer-1A), indicating varying levels of interaction efficiency. (C) Projection of miRNA and
640 mRNA expression values and putative regulatory interactions on the cholesterol biosynthetic
641 pathway.

642

643 **References**

644 Agarwal, V., Bell, G.W., Nam, J.W., and Bartel, D.P. (2015). Predicting effective microRNA target sites in
645 mammalian mRNAs. Elife *4*.
646 Ahluwalia, P.K., Pandey, R.K., Sehajpal, P.K., and Prajapati, V.K. (2017). Perturbed microRNA Expression
647 by Mycobacterium tuberculosis Promotes Macrophage Polarization Leading to Pro-survival Foam Cell.
648 Front Immunol *8*, 107.
649 Amemiya-Kudo, M., Shimano, H., Hasty, A.H., Yahagi, N., Yoshikawa, T., Matsuzaka, T., Okazaki, H.,
650 Tamura, Y., Iizuka, Y., Ohashi, K.*, et al.* (2002). Transcriptional activities of nuclear SREBP-1a, -1c, and -2
651 to different target promoters of lipogenic and cholesterogenic genes. J Lipid Res *43*, 1220-1235.
652 An, W., Yao, S., Sun, X., Hou, Z., Lin, Y., Su, L., and Liu, X. (2019). Glucocorticoid modulatory element-
653 binding protein 1 (GMEB1) interacts with the de-ubiquitinase USP40 to stabilize CFLAR(L) and inhibit
654 apoptosis in human non-small cell lung cancer cells. J Exp Clin Cancer Res *38*, 181.
655 Atri, C., Guerfali, F.Z., and Laouini, D. (2019). MicroRNAs in diagnosis and therapeutics, Vol Chapter 6.
656 Backes, C., Khaleeq, Q.T., Meese, E., and Keller, A. (2016). miEAA: microRNA enrichment analysis and
657 annotation. Nucleic Acids Res *44*, W110-116.
658 Bai, Q., Jin, W., Chen, F., Zhu, J., Cao, L., Yang, Y., Zhong, F., and Li, L. (2024). KLF8 Promotes the Survival
659 of Lung Adenocarcinoma During Nutrient Deprivation by Regulating the Pentose Phosphate Pathway
660 through SIRT2. Front Biosci (Landmark Ed) *29*, 27.
661 Benjamini, Y., and Hochberg, Y. (1995). Controlling the False Discovery Rate: A Practical and Powerful
662 Approach to Multiple Testing. Journal of the Royal Statistical Society: Series B (Methodological) *57*, 289-
663 300.
664 Boleij, A., Fathi, P., Dalton, W., Park, B., Wu, X., Huso, D., Allen, J., Besharati, S., Anders, R.A., Housseau,
665 F.*, et al.* (2021). G-protein coupled receptor 35 (GPR35) regulates the colonic epithelial cell response to
666 enterotoxigenic Bacteroides fragilis. Commun Biol *4*, 585.
667 Brennecke, J., Stark, A., Russell, R.B., and Cohen, S.M. (2005). Principles of microRNA-target recognition.
668 PLoS Biol *3*, e85.
669 Chen, Y., and Wang, X. (2020). miRDB: an online database for prediction of functional microRNA targets.
670 Nucleic Acids Res *48*, D127-D131.
671 Chong, Z.X., Yeap, S.K., and Ho, W.Y. (2021). Unraveling the roles of miRNAs in regulating epithelial-to-
672 mesenchymal transition (EMT) in osteosarcoma. Pharmacol Res *172*, 105818.
673 Conceicao-Silva, F., and Morgado, F.N. (2019). Leishmania Spp-Host Interaction: There Is Always an
674 Onset, but Is There an End? Front Cell Infect Microbiol *9*, 330.
675 Cui, C., hi, B., Shi, J., Zhou, Y., VCui, and Q. (2019). Defining the Importance Score of Human MicroRNAs
676 and Their Single Nucleotide Mutants Using Random Forest Regression and Sequence Data. Adv Theory
677 Simul *2*.
678 de La Llave, E., Lecoeur, H., Besse, A., Milon, G., Prina, E., and Lang, T. (2011). A combined luciferase
679 imaging and reverse transcription polymerase chain reaction assay for the study of Leishmania
680 amastigote burden and correlated mouse tissue transcript fluctuations. Cell Microbiol *13*, 81-91.
681 Denzler, R., McGeary, S.E., Title, A.C., Agarwal, V., Bartel, D.P., and Stoffel, M. (2016). Impact of
682 MicroRNA Levels, Target-Site Complementarity, and Cooperativity on Competing Endogenous RNA-
683 Regulated Gene Expression. Mol Cell *64*, 565-579.
684 Dobin, A., Davis, C.A., Schlesinger, F., Drenkow, J., Zaleski, C., Jha, S., Batut, P., Chaisson, M., and
685 Gingeras, T.R. (2013). STAR: ultrafast universal RNA-seq aligner. Bioinformatics *29*, 15-21.
686 Fernandes, J.C.R., Goncalves, A.N.A., Floeter-Winter, L.M., Nakaya, H.I., and Muxel, S.M. (2022).
687 Comparative transcriptomic analysis of long noncoding RNAs in Leishmania-infected human
688 macrophages. Front Genet *13*, 1051568.

689 Ganguly, S., Ghoshal, B., Banerji, I., Bhattacharjee, S., Chakraborty, S., Goswami, A., Mukherjee, K., and
690 Bhattacharyya, S.N. (2022). Leishmania survives by exporting miR-146a from infected to resident cells to
691 subjugate inflammation. Life Sci Alliance *5*.
692 Geraci, N.S., Tan, J.C., and McDowell, M.A. (2015). Characterization of microRNA expression profiles in
693 Leishmania-infected human phagocytes. Parasite Immunol *37*, 43-51.
694 Golden, R.J., Chen, B., Li, T., Braun, J., Manjunath, H., Chen, X., Wu, J., Schmid, V., Chang, T.C., Kopp, F.*, et*
695 *al.* (2017). An Argonaute phosphorylation cycle promotes microRNA-mediated silencing. Nature *542*,
696 197-202.
697 Griffiths-Jones, S., Grocock, R.J., van Dongen, S., Bateman, A., and Enright, A.J. (2006). miRBase:
698 microRNA sequences, targets and gene nomenclature. Nucleic Acids Res *34*, D140-144.
699 Grimson, A., Farh, K.K., Johnston, W.K., Garrett-Engele, P., Lim, L.P., and Bartel, D.P. (2007). MicroRNA
700 targeting specificity in mammals: determinants beyond seed pairing. Mol Cell *27*, 91-105.
701 Guo, X., Qi, H., Lin, G., Yu, J., Zhang, M., and Gao, X. (2023). ARID3A plays a key regulatory role in palmitic
702 acid-stimulated milk fat synthesis in mouse mammary epithelial cells. Cell Biol Int *47*, 1106-1117.
703 Gutierrez Sanchez, M., Zhang, S., Gharsallah, C., Lamotte, S., Varet, H., Legendre, R., Dingli, F., Loew, D.,
704 Rotili, D., Valente, S.*, et al.* (2023). Inhibition of the macrophage demethylase LSD1 reverses Leishmania
705 amazonensis-induced transcriptomic changes and causes a decrease in parasite load. BioRxiv
706 *doi.org/10.1101/2023.09.29.560133*
707 Hauptmann, J., Schraivogel, D., Bruckmann, A., Manickavel, S., Jakob, L., Eichner, N., Pfaff, J., Urban, M.,
708 Sprunck, S., Hafner, M.*, et al.* (2015). Biochemical isolation of Argonaute protein complexes by Ago-APP.
709 Proc Natl Acad Sci U S A *112*, 11841-11845.
710 Kamhawi, S., and Serafim, T.D. (2020). Leishmania: A Maestro in Epigenetic Manipulation of Macrophage
711 Inflammasomes. Trends Parasitol *36*, 498-501.
712 Kao, T.W., Chen, H.H., Lin, J., Wang, T.L., and Shen, Y.A. (2024). PBX1 as a novel master regulator in
713 cancer: Its regulation, molecular biology, and therapeutic applications. Biochim Biophys Acta Rev Cancer
714 *1879*, 189085.
715 Kozomara, A., Birgaoanu, M., and Griffiths-Jones, S. (2019). miRBase: from microRNA sequences to
716 function. Nucleic Acids Res *47*, D155-D162.
717 Krek, A., Grun, D., Poy, M.N., Wolf, R., Rosenberg, L., Epstein, E.J., MacMenamin, P., da Piedade, I.,
718 Gunsalus, K.C., Stoffel, M.*, et al.* (2005). Combinatorial microRNA target predictions. Nat Genet *37*, 495-
719 500.
720 Kruger, J., and Rehmsmeier, M. (2006). RNAhybrid: microRNA target prediction easy, fast and flexible.
721 Nucleic Acids Res *34*, W451-454.
722 Lambert, S.A., Jolma, A., Campitelli, L.F., Das, P.K., Yin, Y., Albu, M., Chen, X., Taipale, J., Hughes, T.R., and
723 Weirauch, M.T. (2018). The Human Transcription Factors. Cell *172*, 650-665.
724 Langmead, B., Trapnell, C., Pop, M., and Salzberg, S.L. (2009). Ultrafast and memory-efficient alignment
725 of short DNA sequences to the human genome. Genome Biol *10*, R25.
726 Larivera, S., Neumeier, J., and Meister, G. (2023). Post-transcriptional gene silencing in a dynamic RNP
727 world. Biol Chem *404*, 1051-1067.
728 Lecoeur, H., Prina, E., Gutierrez-Sanchez, M., and Spath, G.F. (2022a). Going ballistic: Leishmania nuclear
729 subversion of host cell plasticity. Trends Parasitol *38*, 205-216.
730 Lecoeur, H., Prina, E., Rosazza, T., Kokou, K., N'Diaye, P., Aulner, N., Varet, H., Bussotti, G., Xing, Y., Milon,
731 G.*, et al.* (2020a). Targeting Macrophage Histone H3 Modification as a Leishmania Strategy to Dampen
732 the NF-kappaB/NLRP3-Mediated Inflammatory Response. Cell Rep *30*, 1870-1882 e1874.
733 Lecoeur, H., Rosazza, T., Kokou, K., Varet, H., Coppee, J.Y., Lari, A., Commere, P.H., Weil, R., Meng, G.,
734 Milon, G.*, et al.* (2020b). Leishmania amazonensis Subverts the Transcription Factor Landscape in
735 Dendritic Cells to Avoid Inflammasome Activation and Stall Maturation. Front Immunol *11*, 1098.

736 Lecoeur, H., Zhang, S., Varet, H., Legendre, R., Proux, C., Granjean, C., Bousso, P., Prina, E., and Späth,
737 G.F. (2022b). *Leishmania amazonensis* controls macrophage-regulated cell death to establish chronic
738 infection *in vitro* and *in vivo*. bioRxiv, 2022.2009.2014.507851.
739 Lemaire, J., Mkannez, G., Guerfali, F.Z., Gustin, C., Attia, H., Sghaier, R.M., Sysco, C., Dellagi, K., Laouini,
740 D., and Renard, P. (2013). MicroRNA expression profile in human macrophages in response to
741 Leishmania major infection. PLoS Negl Trop Dis *7*, e2478.
742 Lewis, B.P., Burge, C.B., and Bartel, D.P. (2005). Conserved seed pairing, often flanked by adenosines,
743 indicates that thousands of human genes are microRNA targets. Cell *120*, 15-20.
744 Lewis, B.P., Shih, I.H., Jones-Rhoades, M.W., Bartel, D.P., and Burge, C.B. (2003). Prediction of
745 mammalian microRNA targets. Cell *115*, 787-798.
746 Li, T., Wu, M., Zhu, Y.Y., Chen, J., and Chen, L. (2014). Development of RNA interference-based
747 therapeutics and application of multi-target small interfering RNAs. Nucleic Acid Ther *24*, 302-312.
748 Liao, Y., Smyth, G.K., and Shi, W. (2014). featureCounts: an efficient general purpose program for
749 assigning sequence reads to genomic features. Bioinformatics *30*, 923-930.
750 Litvak-Greenfeld, D., and Benhar, I. (2012). Risks and untoward toxicities of antibody-based
751 immunoconjugates. Adv Drug Deliv Rev *64*, 1782-1799.
752 Liu, Q., Novak, M.K., Pepin, R.M., Eich, T., and Hu, W. (2021). microRNA-mediated regulation of
753 microRNA machinery controls cell fate decisions. Elife *10*.
754 Loh, X.Y., Sun, Q.Y., Ding, L.W., Mayakonda, A., Venkatachalam, N., Yeo, M.S., Silva, T.C., Xiao, J.F., Doan,
755 N.B., Said, J.W.*, et al.* (2020). RNA-Binding Protein ZFP36L1 Suppresses Hypoxia and Cell-Cycle Signaling.
756 Cancer Res *80*, 219-233.
757 Lorenz, R., Bernhart, S.H., Honer Zu Siederdissen, C., Tafer, H., Flamm, C., Stadler, P.F., and Hofacker, I.L.
758 (2011). ViennaRNA Package 2.0. Algorithms Mol Biol *6*, 26.
759 Love, M.I., Huber, W., and Anders, S. (2014). Moderated estimation of fold change and dispersion for
760 RNA-seq data with DESeq2. Genome Biol *15*, 550.
761 Luna, J.M., Scheel, T.K., Danino, T., Shaw, K.S., Mele, A., Fak, J.J., Nishiuchi, E., Takacs, C.N., Catanese,
762 M.T., de Jong, Y.P.*, et al.* (2015). Hepatitis C virus RNA functionally sequesters miR-122. Cell *160*, 1099-
763 1110.
764 Marr, A.K., MacIsaac, J.L., Jiang, R., Airo, A.M., Kobor, M.S., and McMaster, W.R. (2014). Leishmania
765 donovani infection causes distinct epigenetic DNA methylation changes in host macrophages. PLoS
766 Pathog *10*, e1004419.
767 Martinez-Hernandez, J.E., Hammoud, Z., de Sousa, A.M., Kramer, F., Monte-Neto, R.L.D., Maracaja-
768 Coutinho, V., and Martin, A.J.M. (2021). Network-Based Approaches Reveal Potential Therapeutic
769 Targets for Host-Directed Antileishmanial Therapy Driving Drug Repurposing. Microbiol Spectr *9*,
770 e0101821.
771 Mauro, M., Berretta, M., Palermo, G., Cavalieri, V., and La Rocca, G. (2023). The Multiplicity of Argonaute
772 Complexes in Mammalian Cells. J Pharmacol Exp Ther *384*, 1-9.
773 McGeary, S.E., Lin, K.S., Shi, C.Y., Pham, T.M., Bisaria, N., Kelley, G.M., and Bartel, D.P. (2019). The
774 biochemical basis of microRNA targeting efficacy. Science *366*.
775 McGwire, B.S., and Satoskar, A.R. (2014). Leishmaniasis: clinical syndromes and treatment. QJM *107*, 7-
776 14.
777 Mishra, R., Mohanty, S., Mahapatra, S., and Prasad, P. (2023). Overview of microbial therapeutics in
778 immunological disorders. Microbiome Therapeutics, 289-353.
779 Mukherjee, B., Paul, J., Mukherjee, S., Mukhopadhyay, R., Das, S., Naskar, K., Sundar, S., Dujardin, J.C.,
780 Saha, B., and Roy, S. (2015). Antimony-Resistant Leishmania donovani Exploits miR-466i To Deactivate
781 Host MyD88 for Regulating IL-10/IL-12 Levels during Early Hours of Infection. J Immunol *195*, 2731-2742.
782 Murdaca, G., Tonacci, A., Negrini, S., Greco, M., Borro, M., Puppo, F., and Gangemi, S. (2019). Effects of
783 AntagomiRs on Different Lung Diseases in Human, Cellular, and Animal Models. Int J Mol Sci *20*.

784 Muxel, S.M., Acuna, S.M., Aoki, J.I., Zampieri, R.A., and Floeter-Winter, L.M. (2018). Toll-Like Receptor
785 and miRNA-let-7e Expression Alter the Inflammatory Response in Leishmania amazonensis-Infected
786 Macrophages. Front Immunol *9*, 2792.
787 Muxel, S.M., Laranjeira-Silva, M.F., Zampieri, R.A., and Floeter-Winter, L.M. (2017). Leishmania
788 (Leishmania) amazonensis induces macrophage miR-294 and miR-721 expression and modulates
789 infection by targeting NOS2 and L-arginine metabolism. Sci Rep *7*, 44141.
790 Nandan, D., Rath, C.T., and Reiner, N.E. (2021). Leishmania regulates host macrophage miRNAs
791 expression by engaging transcription factor c-Myc. J Leukoc Biol *109*, 999-1007.
792 Osorio y Fortea, J., de La Llave, E., Regnault, B., Coppee, J.Y., Milon, G., Lang, T., and Prina, E. (2009).
793 Transcriptional signatures of BALB/c mouse macrophages housing multiplying Leishmania amazonensis
794 amastigotes. BMC Genomics *10*, 119.
795 Pasquinelli, A.E., Reinhart, B.J., Slack, F., Martindale, M.Q., Kuroda, M.I., Maller, B., Hayward, D.C., Ball,
796 E.E., Degnan, B., Muller, P.*, et al.* (2000). Conservation of the sequence and temporal expression of let-7
797 heterochronic regulatory RNA. Nature *408*, 86-89.
798 Patterson, E.S., Addis, R.C., Shamblott, M.J., and Gearhart, J.D. (2008). SOX17 directly activates Zfp202
799 transcription during in vitro endoderm differentiation. Physiol Genomics *34*, 277-284.
800 Pikuleva, I.A., Babiker, A., Waterman, M.R., and Bjorkhem, I. (1998). Activities of recombinant human
801 cytochrome P450c27 (CYP27) which produce intermediates of alternative bile acid biosynthetic
802 pathways. J Biol Chem *273*, 18153-18160.
803 Popenda, M., Szachniuk, M., Antczak, M., Purzycka, K.J., Lukasiak, P., Bartol, N., Blazewicz, J., and
804 Adamiak, R.W. (2012). Automated 3D structure composition for large RNAs. Nucleic Acids Res *40*, e112.
805 Quazi, F., and Molday, R.S. (2013). Differential phospholipid substrates and directional transport by ATP-
806 binding cassette proteins ABCA1, ABCA7, and ABCA4 and disease-causing mutants. J Biol Chem *288*,
807 34414-34426.
808 Quevillon Huberdeau, M., Zeitler, D.M., Hauptmann, J., Bruckmann, A., Fressigne, L., Danner, J., Piquet,
809 S., Strieder, N., Engelmann, J.C., Jannot, G.*, et al.* (2017). Phosphorylation of Argonaute proteins affects
810 mRNA binding and is essential for microRNA-guided gene silencing in vivo. EMBO J *36*, 2088-2106.
811 R-Core-Team (2016). R: A Language and Environment for Statistical Computing. R Foundation for
812 Statistical Computing. https://wwwR-projectorg/.
813 Ramos-Sanchez, E.M., Reis, L.C., Souza, M.A., Muxel, S.M., Santos, K.R., Lagos, D., Pereira, V.R.A., de
814 Brito, M.E.F., Kaye, P.M., Floeter-Winter, L.M.*, et al.* (2022). miR-548d-3p Is Up-Regulated in Human
815 Visceral Leishmaniasis and Suppresses Parasite Growth in Macrophages. Front Cell Infect Microbiol *12*,
816 826039.
817 Rashidi, S., Mansouri, R., Ali-Hassanzadeh, M., Ghani, E., Barazesh, A., Karimazar, M., Nguewa, P., and
818 Carrera Silva, E.A. (2021). Highlighting the interplay of microRNAs from Leishmania parasites and
819 infected-host cells. Parasitology *148*, 1434-1446.
820 Riolo, G., Cantara, S., Marzocchi, C., and Ricci, C. (2020). miRNA Targets: From Prediction Tools to
821 Experimental Validation. Methods Protoc *4*.
822 Rupaimoole, R., and Slack, F.J. (2017). MicroRNA therapeutics: towards a new era for the management of
823 cancer and other diseases. Nat Rev Drug Discov *16*, 203-222.
824 Shalgi, R., Lieber, D., Oren, M., and Pilpel, Y. (2007). Global and local architecture of the mammalian
825 microRNA-transcription factor regulatory network. PLoS Comput Biol *3*, e131.
826 Shannon, P., Markiel, A., Ozier, O., Baliga, N.S., Wang, J.T., Ramage, D., Amin, N., Schwikowski, B., and
827 Ideker, T. (2003). Cytoscape: a software environment for integrated models of biomolecular interaction
828 networks. Genome Res *13*, 2498-2504.
829 Smith, T., Heger, A., and Sudbery, I. (2017). UMI-tools: modeling sequencing errors in Unique Molecular
830 Identifiers to improve quantification accuracy. Genome Res *27*, 491-499.

831 Spath, G.F., Schlesinger, P., Schreiber, R., and Beverley, S.M. (2009). A novel role for Stat1 in phagosome
832 acidification and natural host resistance to intracellular infection by Leishmania major. PLoS Pathog *5*,
833 e1000381.
834 Sprenkle, N.T., Serezani, C.H., and Pua, H.H. (2023). MicroRNAs in Macrophages: Regulators of Activation
835 and Function. J Immunol *210*, 359-368.
836 Sun, X., Hua, S., Chen, H.R., Ouyang, Z., Einkauf, K., Tse, S., Ard, K., Ciaranello, A., Yawetz, S., Sax, P.*, et al.*
837 (2017). Transcriptional Changes during Naturally Acquired Zika Virus Infection Render Dendritic Cells
838 Highly Conducive to Viral Replication. Cell Rep *21*, 3471-3482.
839 Supek, F., Bosnjak, M., Skunca, N., and Smuc, T. (2011). REVIGO summarizes and visualizes long lists of
840 gene ontology terms. PLoS One *6*, e21800.
841 Taghehchian, N., Samsami, Y., Maharati, A., Zangouei, A.S., Boroumand-Noughabi, S., and Moghbeli, M.
842 (2023). Molecular biology of microRNA-342 during tumor progression and invasion. Pathol Res Pract *248*,
843 154672.
844 Tai, M.C., Kajino, T., Nakatochi, M., Arima, C., Shimada, Y., Suzuki, M., Miyoshi, H., Yatabe, Y.,
845 Yanagisawa, K., and Takahashi, T. (2015). miR-342-3p regulates MYC transcriptional activity via direct
846 repression of E2F1 in human lung cancer. Carcinogenesis *36*, 1464-1473.
847 Thammaiah, C.K., and Jayaram, S. (2016). Role of let-7 family microRNA in breast cancer. Noncoding RNA
848 Res *1*, 77-82.
849 Tiwari, N., Kumar, V., Gedda, M.R., Singh, A.K., Singh, V.K., Gannavaram, S., Singh, S.P., and Singh, R.K.
850 (2017). Identification and Characterization of miRNAs in Response to Leishmania donovani Infection:
851 Delineation of Their Roles in Macrophage Dysfunction. Front Microbiol *8*, 314.
852 Trimarchi, J.M., Fairchild, B., Wen, J., and Lees, J.A. (2001). The E2F6 transcription factor is a component
853 of the mammalian Bmi1-containing polycomb complex. Proc Natl Acad Sci U S A *98*, 1519-1524.
854 Tsang, J., Zhu, J., and van Oudenaarden, A. (2007). MicroRNA-mediated feedback and feedforward loops
855 are recurrent network motifs in mammals. Mol Cell *26*, 753-767.
856 Valinezhad Orang, A., Safaralizadeh, R., and Kazemzadeh-Bavili, M. (2014). Mechanisms of miRNA-
857 Mediated Gene Regulation from Common Downregulation to mRNA-Specific Upregulation. Int J
858 Genomics *2014*, 970607.
859 Wang, T., Zhou, T., Fu, F., Han, Y., Li, Y., and Yuan, M. (2022). HMGA1 As a Potential Prognostic and
860 Therapeutic Biomarker in Breast Cancer. Dis Markers *2022*, 7466555.
861 Xu, L., Wang, Z., and Wang, G. (2024). Screening of Biomarkers Associated with Osteoarthritis Aging
862 Genes and Immune Correlation Studies. Int J Gen Med *17*, 205-224.
863 Zeng, Y., Sankala, H., Zhang, X., and Graves, P.R. (2008). Phosphorylation of Argonaute 2 at serine-387
864 facilitates its localization to processing bodies. Biochem J *413*, 429-436.
865 Zhang, L., Guo, H., Zhang, X., Wang, L., Wei, F., Zhao, Y., Wang, B., Meng, Y., and Li, Y. (2024). Small
866 nucleolar RNA Snora73 promotes psoriasis progression by sponging miR-3074-5p and regulating PBX1
867 expression. Funct Integr Genomics *24*, 15.
868 Zhang, P., Wu, W., Chen, Q., and Chen, M. (2019). Non-Coding RNAs and their Integrated Networks. J
869 Integr Bioinform *16*.
870 Zhang, S., Lecoeur, H., Varet, H., Legendre, R., Mahtal, N., Proux, C., Aulner, N., Shorte, S., Granjean, C.,
871 Bousso, P.*, et al.* (2022). Immunometabolic profiling of in vitro and ex vivo *Leishmania*-infected
872 macrophages (LIMs) reveals unique polarization and bioenergetic signatures. BioRxiv,
873 2022.2009.2008.507100.

874

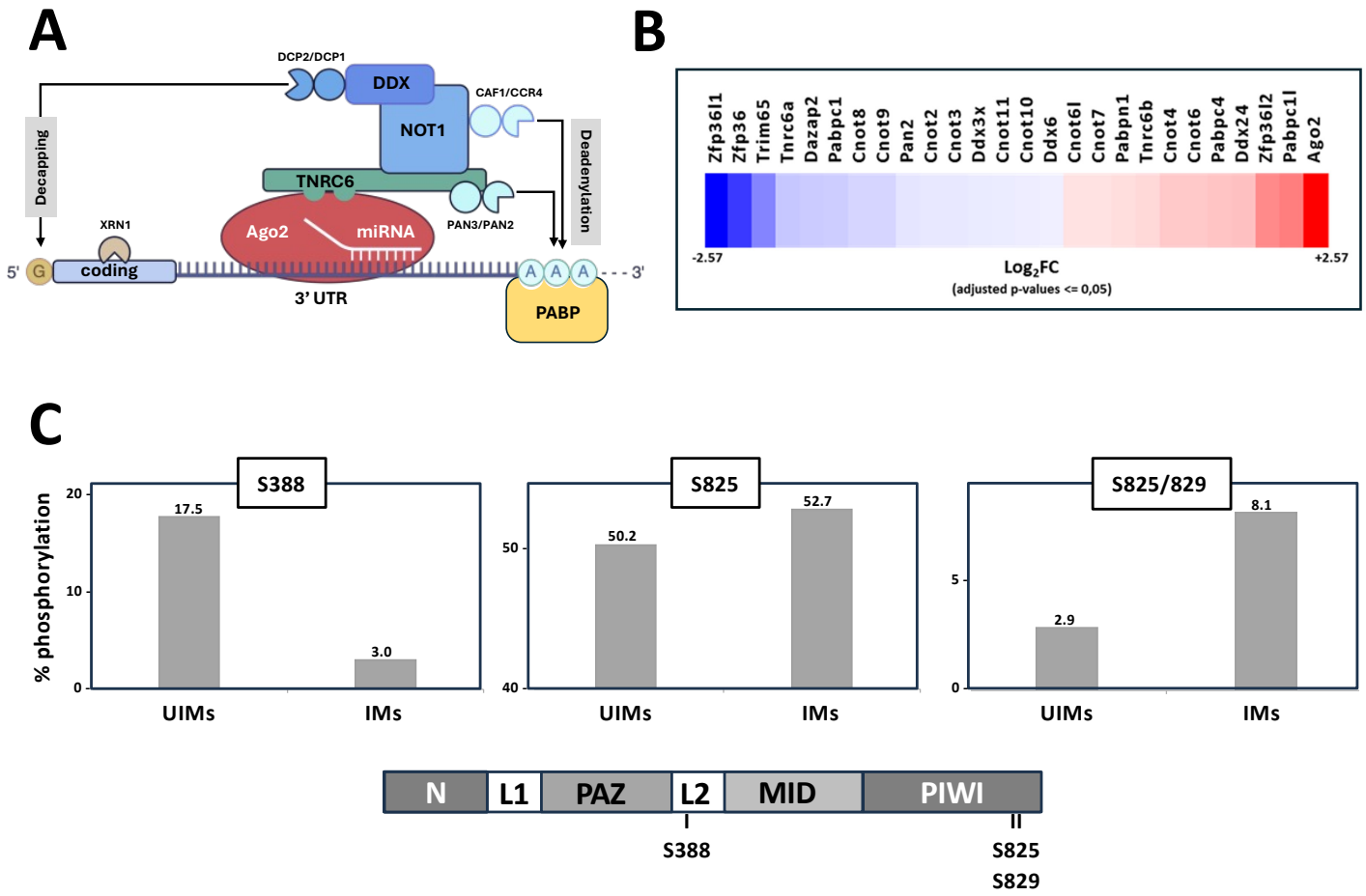

FIGURE 1, Gharsallah et al.

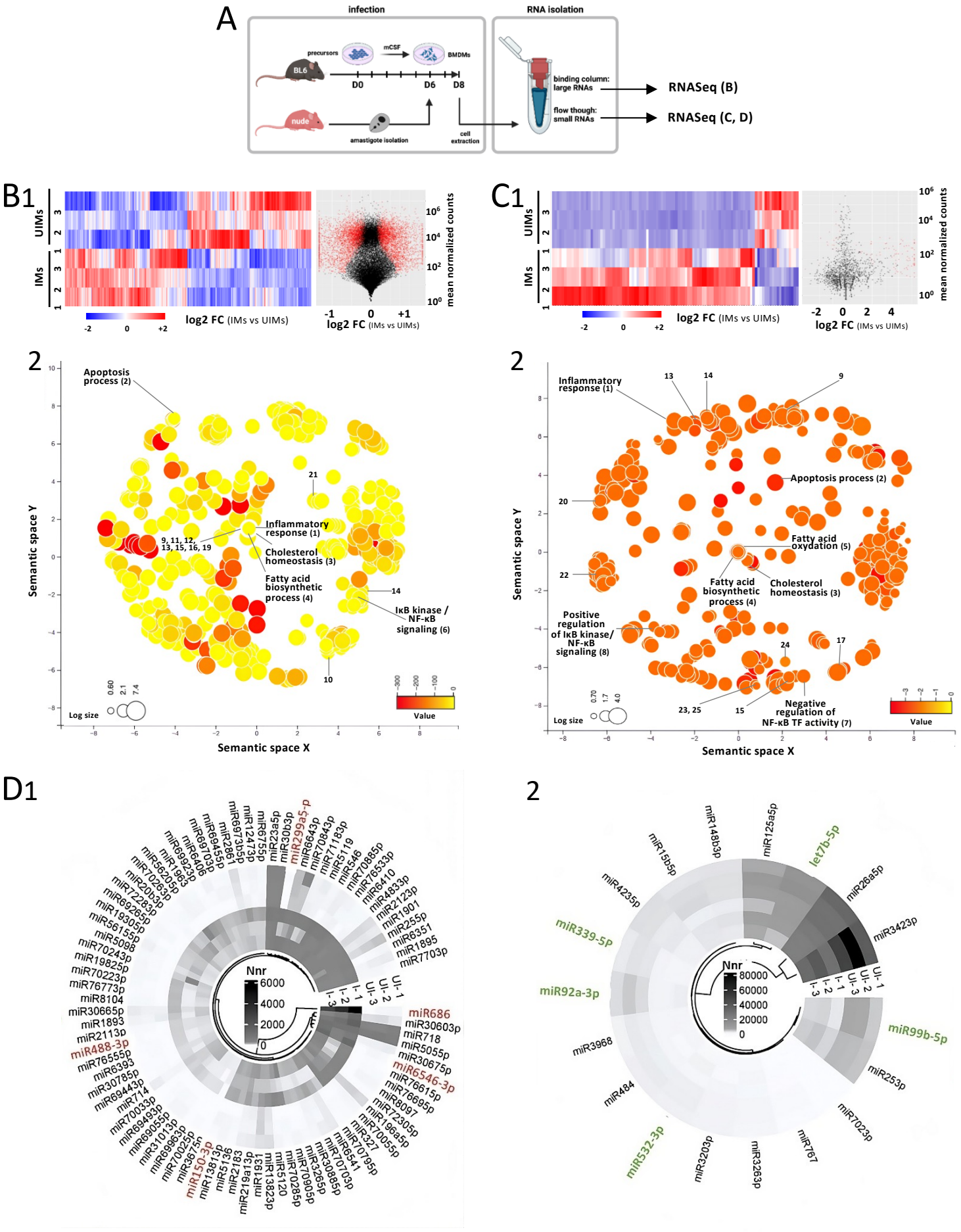

FIGURE 2, Gharsallah et al.

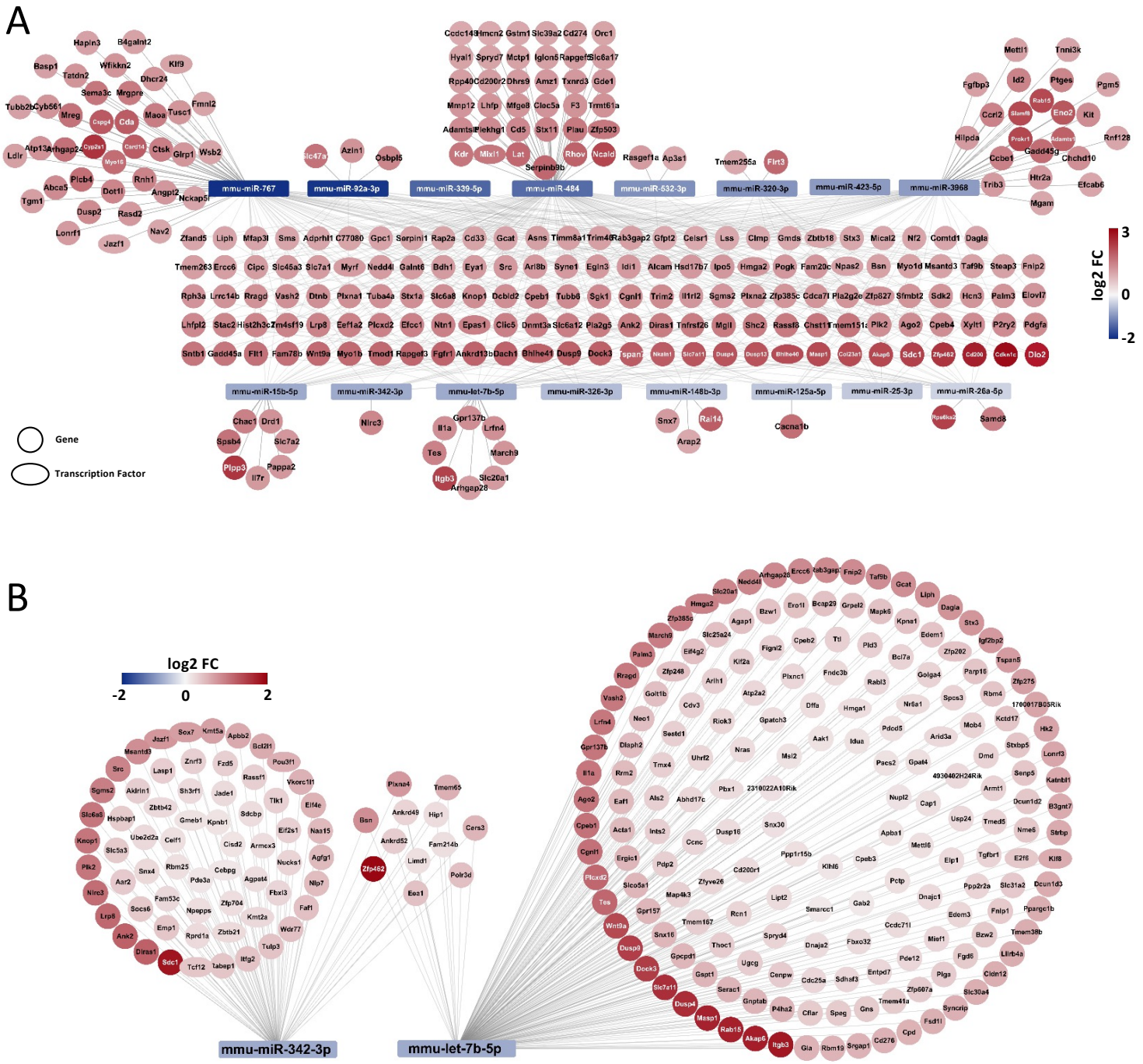

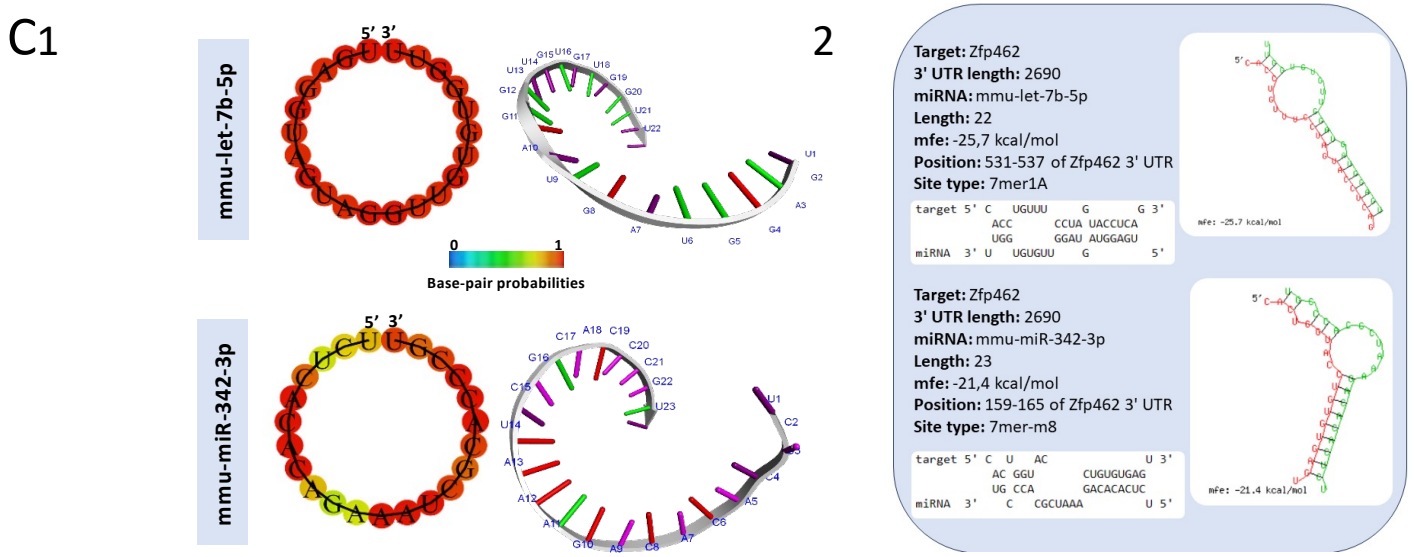

FIGURE 3, Gharsallah et al.

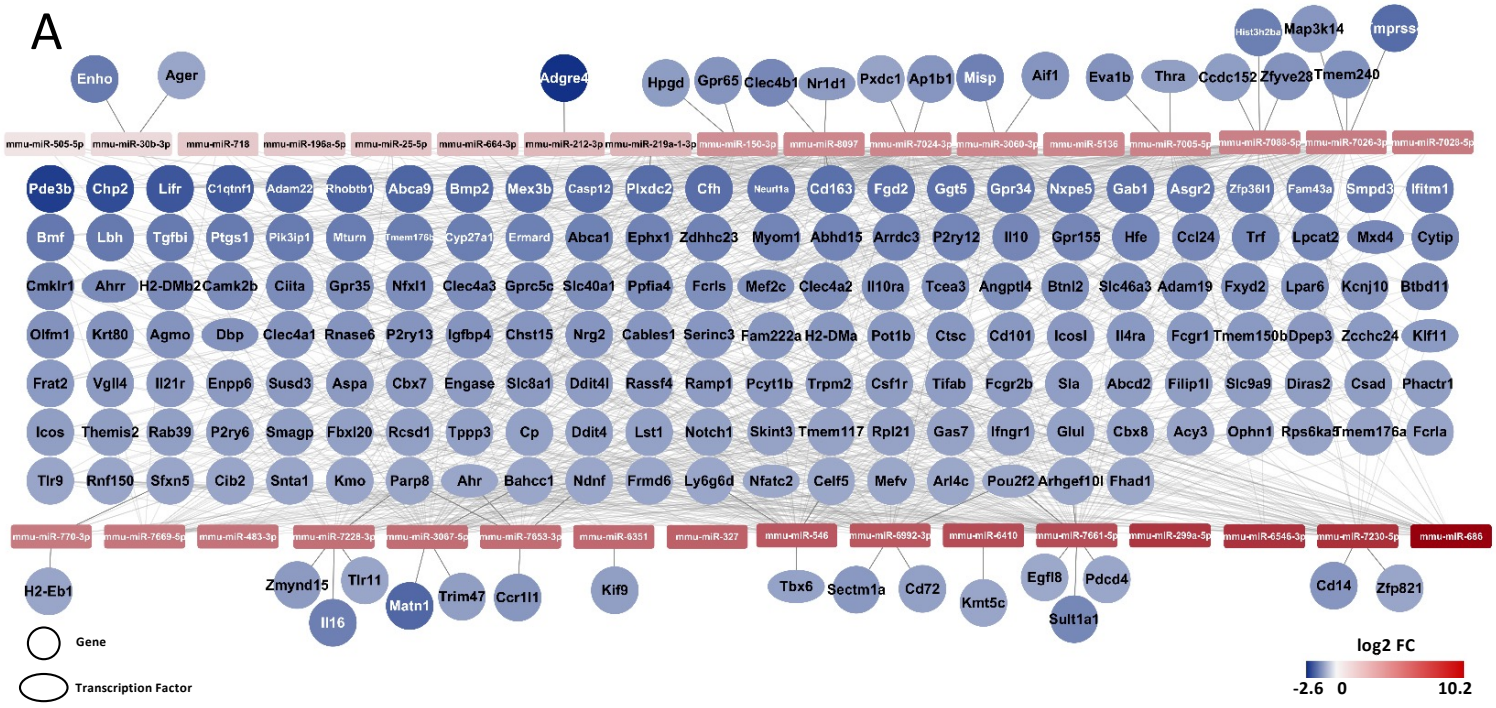

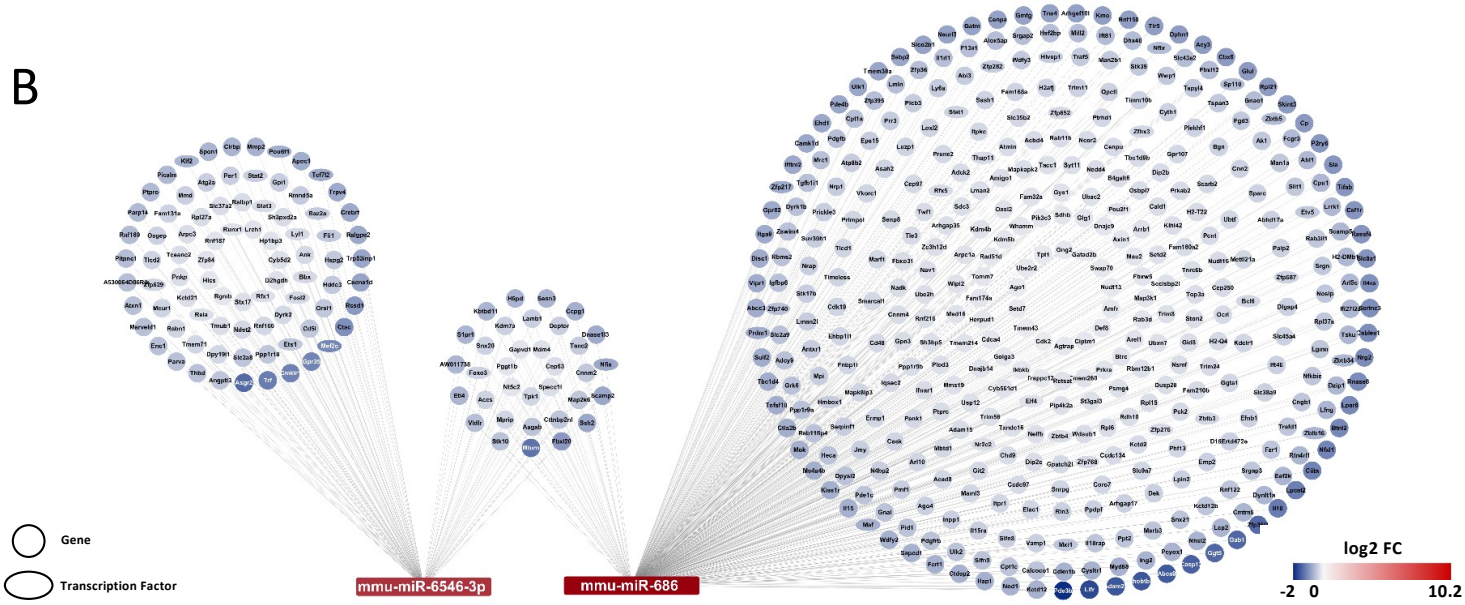

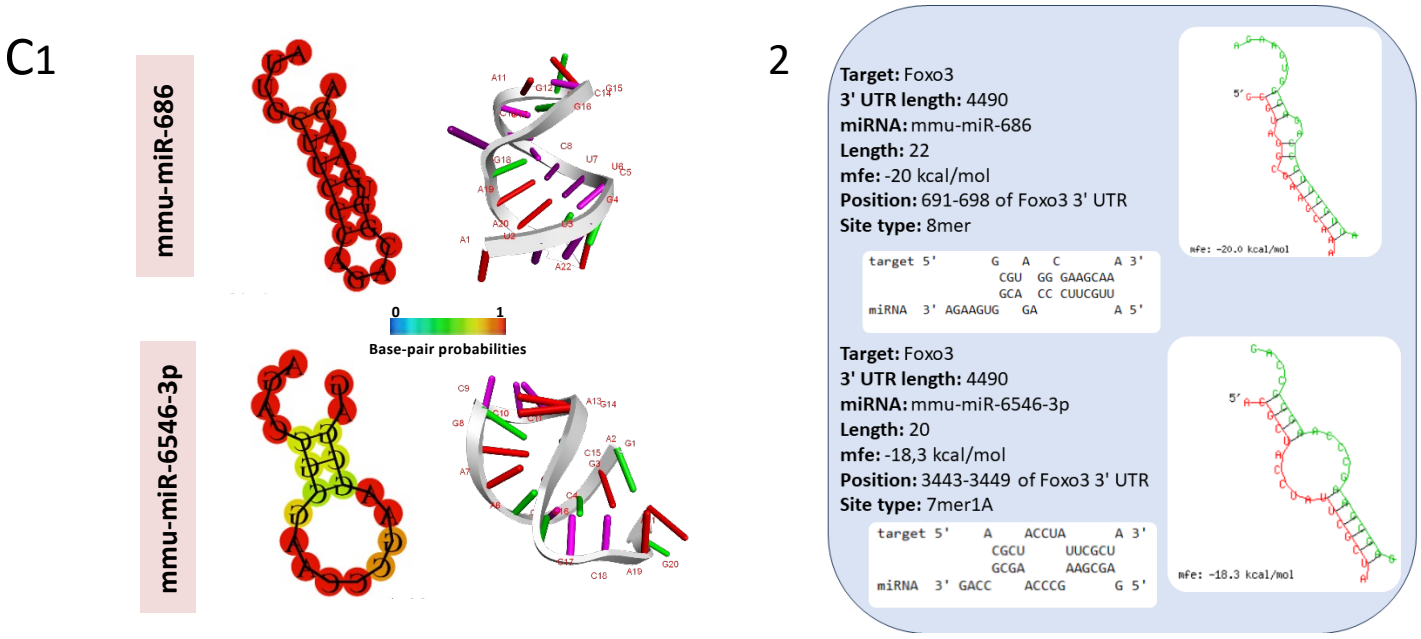

FIGURE 4, Gharsallah et al.

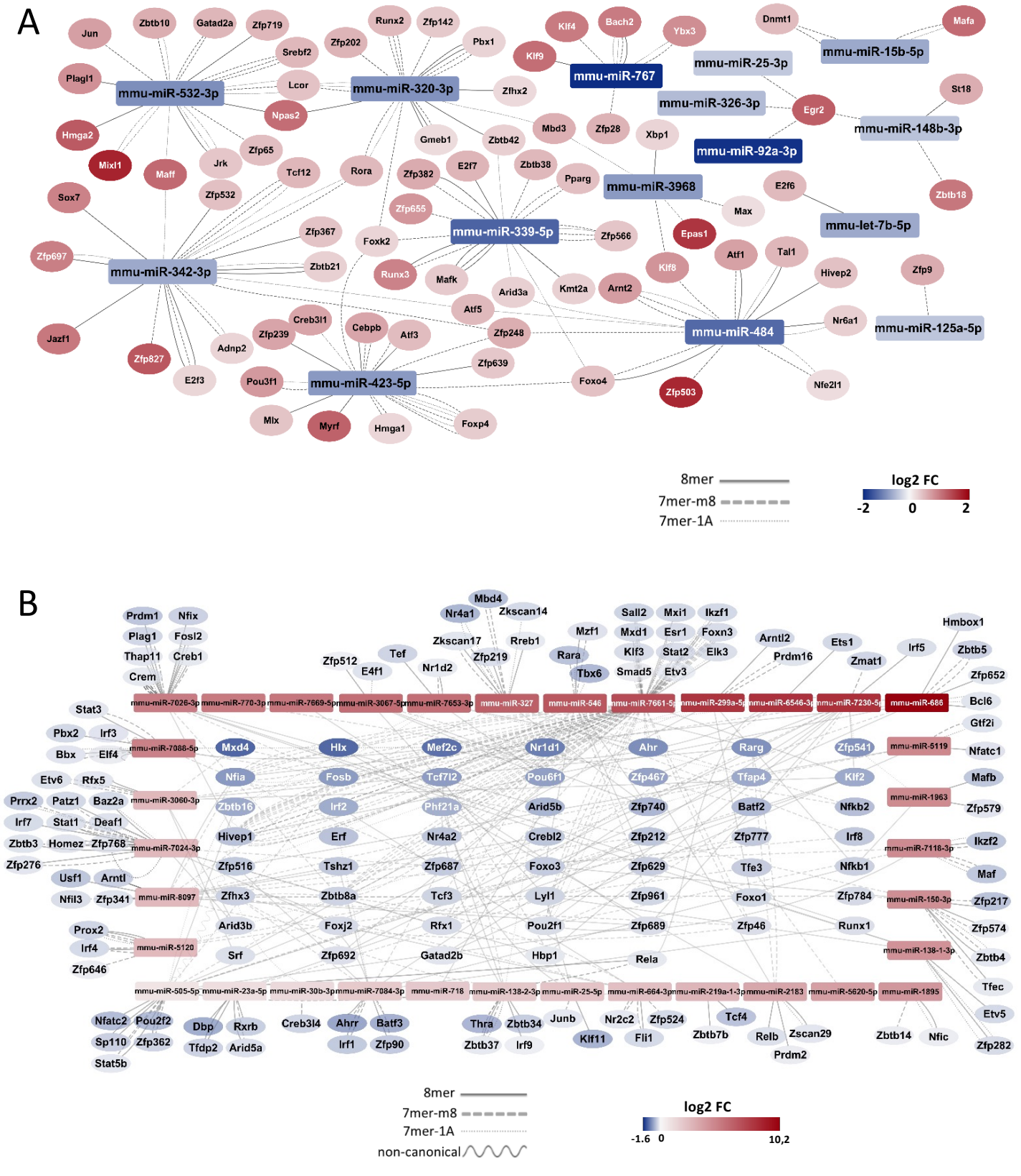

FIGURE 5, Gharsallah et al.

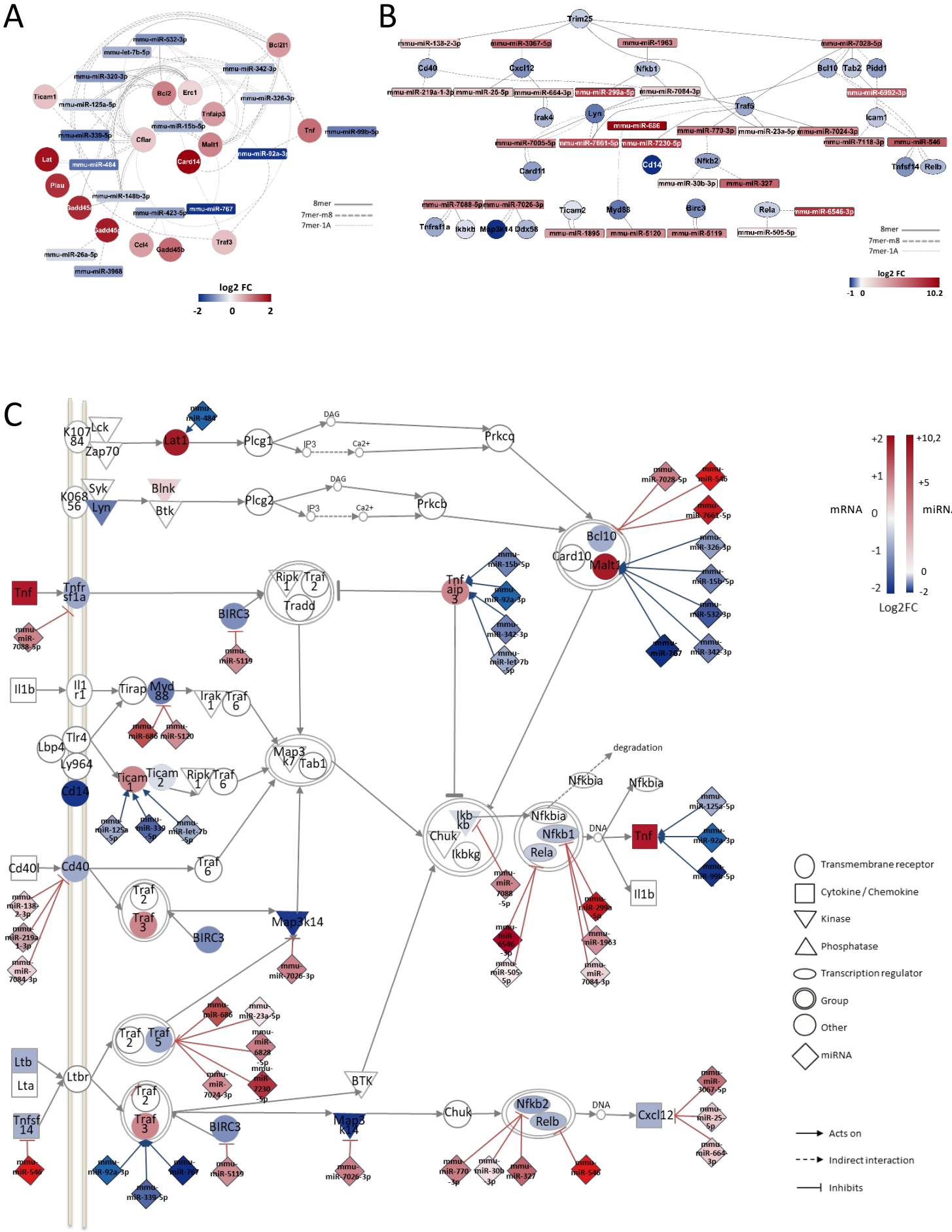

FIGURE 6, Gharsallah et al.

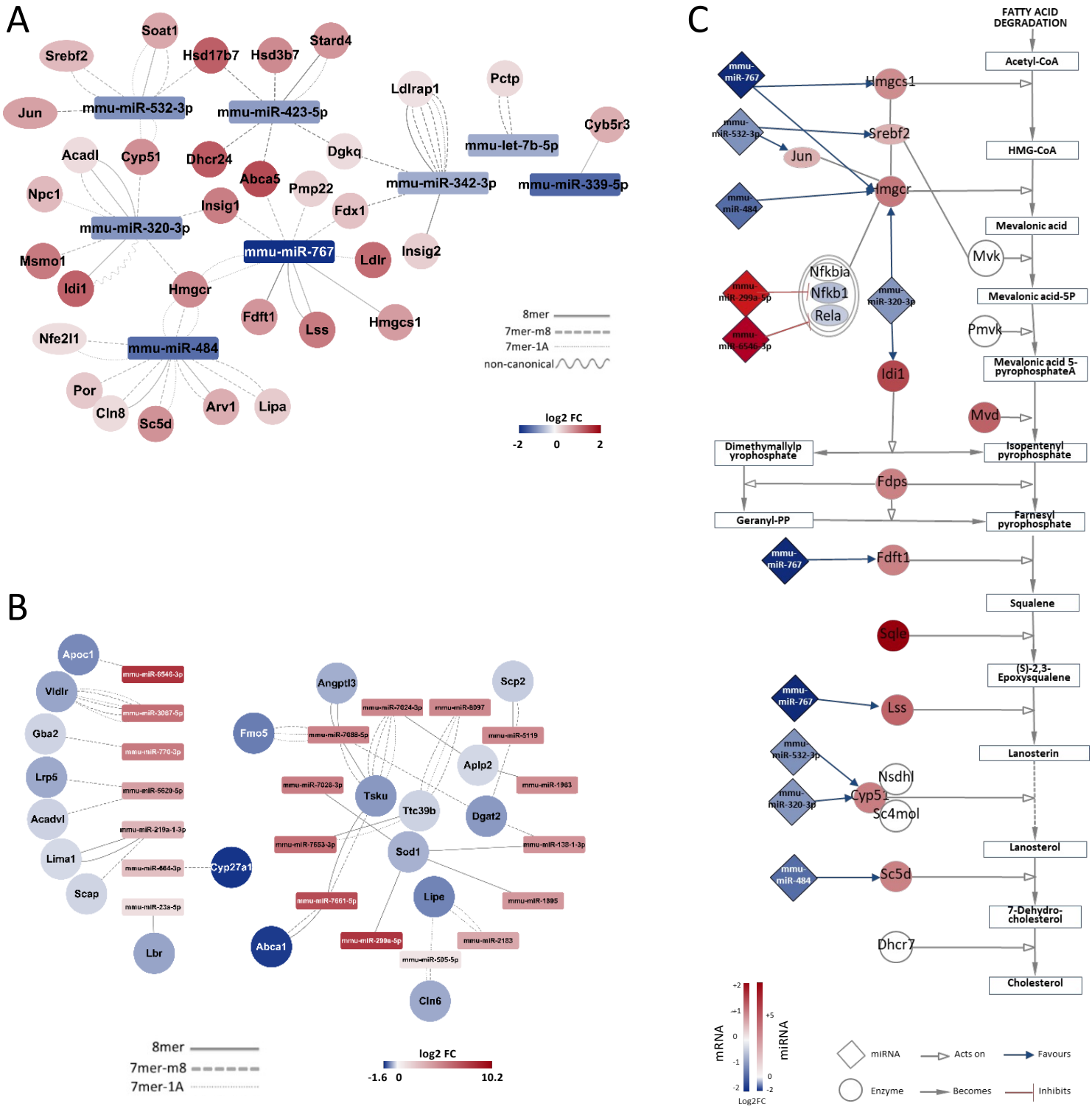

FIGURE 7, Gharsallah et al.